Taylor & Francis
Taylor & Francis Group

FOCUS ISSUE REVIEW

∂ OPEN ACCESS 	Check for updates

Atomic force microscopy for characterization of decellularized extracellular matrix (dECM) based materials

Svetlana Batasheva [a,b], Svetlana Kotova [a], Anastasia Frolova [a] and Rawil Fakhrullin [a,b]

aInstitute for Regenerative Medicine, Sechenov First Moscow State Medical University (Sechenov University), Moscow, Russian Federation; bInstitute of Fundamental Medicine and Biology, Kazan Federal University, Republic of Tatarstan Kazan, Russian Federation

ABSTRACT

In live organisms, cells are embedded in tissue-specific extracellular matrix (ECM), which provides chemical and mechanical signals important for cell differentiation, migration, and overall functionality. Careful reproduction of ECM properties in artificial cell scaffolds is necessary to get physiologically relevant results of in vitro studies and produce robust materials for cell and tissue engineering. Nanoarchitectonics is a contemporary way to building complex materials from nano-scale objects of artificial and biological origin. Decellularized ECM (dECM), remaining after cell elimination from organs, tissues and cell cultures is arguably the closest equivalent of native ECM achievable today. dECM-based materials can be used as templates or components for producing cell scaffolds using nanoarchitectonic approach. Irrespective of the form, in which dECM is used (whole acellular organ/tissue, bioink or hydrogel), the local stiffness of the dECM scaffold must be evaluated, since the fate of seeded cells depends on the mechanical properties of their environment. Careful dECM characterization is also necessary to reproduce essential ECM traits in artificial cell scaffolds by nanoparticle assembly. Atomic force microscopy (AFM) is a valuable characterization tool, as it allows simultaneous assessment of mechanical and topographic features of the scaffold, and additionally evaluate the efficiency of decellularization process and preservation of the extracellular matrix. This review depicts the current application of AFM in the field of dECM-based materials, including the basics of AFM technique and the use of flicker-noise spectroscopy (FNS) method for the quantification of the dECM micro- and nanostructure.
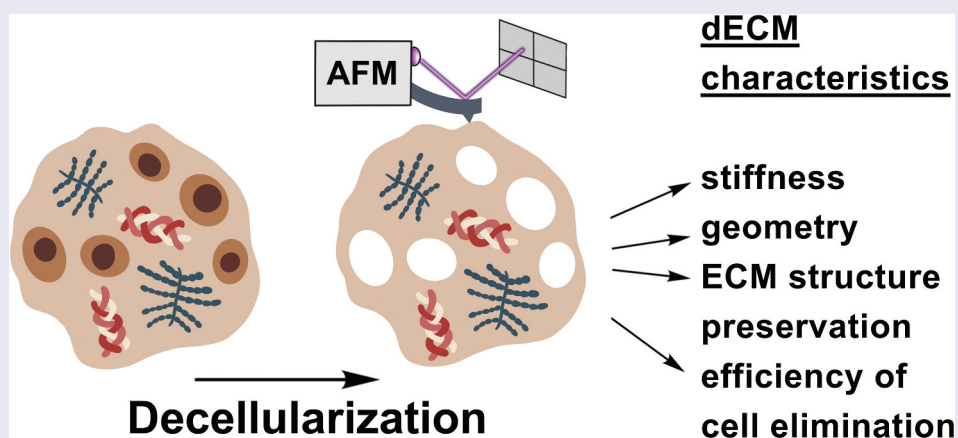
IMPACT STATEMENT

Although several reviews on different aspects of dECM-based materials have been published recently, current applications of AFM to characterizing dECM-based scaffolds have not been summarized in specialized reviews since 2017.

1. Introduction

In recent years, artificial cell substrates have evolved from flat-bottom Petri dishes to structurally elaborated cell scaffolds obtained from moulded synthetic polymers and compound biomaterials. Cultivating cells in vitro as a monolayer culture is a relatively cheap and simple procedure widely used in scientific research. However, it has become evident that in vitro grown monolayer cells significantly differ from their counterparts in vivo, because they do not receive certain specific chemical and physical signals characteristic of the source

tissue. Within the organism, cells are surrounded by extracellular matrix (ECM), which is a complex material consisting of fibrous and gel-like components having a tissue-specific composition [1]. ECM provides specific stimuli that are crucially important for cell differentiation, proliferation, and eventually survival. To supply the cells with ECM-derived signals, various approaches can be used. Some of them reproduce the mechanical and chemical properties of the cell environment with synthetic moulds equipped with conjugated signalling molecules [2]. An alternative approach relies on the use of decellularized ECM (dECM) of cell cultures, tissues and whole organs as a material for producing cell scaffolds [3,4] because it can potentially provide the whole set of natural signals familiar to the cell. Cell propagation under conditions closely resembling the native ones is crucially important for both tissue engineering and relevant in vitro research. As such, the dECM-based materials play an important role in biological micromanufacturing.

Nanoarchitectonics is a novel approach for material design, which often benefits from complex architecture and rich chemistry of biological objects to synthesize and/or assemble nanoparticles [5]. Bio-objects can be used as either templates or components for producing materials for tissue engineering using nanoarchitectural approach [6]. Some individual ECM constituents such as hyaluronic acid [7], fibronectin [8] and collagens [9,10] have been applied as building blocks for biomaterials capable of modulating cellular behaviours. Nanoarchitectonics allows obtaining synthetic, bioartificial or composite cell scaffolds, but irrespective of the differences in composition and manufacture procedures, all the scaffolds eventually try to mimic the properties of the natural cell supports [11,12]. Characterisation methods at the nanoscale are an important part of virtually every nanoarchitectonics study.

Atomic force microscopy (AFM) is a valuable tool for characterising the physical properties of cell scaffolds, allowing both observing topography and registering mechanical properties of materials at the micro- and nano-level. Although transmission and scanning electron microscopy techniques can be also applied to study dECM substrate topography with high resolution, these methods can be more destructive to ECM structure, because they require chemical fixation and staining of a specimen, and exploit high energy electron beams for imaging [13]. In contrast to these methods, AFM imaging is not destructive and may be performed on non-fixed and non-stained samples [13] and in liquid to imitate the conditions in the living cells [14]. AFM analysis may be followed by histological examination to identify the chemical composition of specific regions of interest [13]. The use of AFM for analysing dECM from various tissues can

contribute to studies of the structure-function relationships in different tissues at both micrometre and nanometre scales. Several excellent reviews on dECM scaffolds generation and applications have been published recently [3,4,15,16]. However, the reviews on AFM application to dECM characterization are limited by few papers [14,17]. This review describes the general principles of AFM data acquisition and treatment, and current application of AFM in the field of dECM-based materials.

2. General principles of AFM data acquisition

Atomic force microscopy is a high-resolution method of visualization of different surfaces such as cells, single molecules, viruses, collagen structures and polymer materials [18–21]. AFM also enables obtaining data on the mechanical properties of the object surface, using a range of versatile imaging modes [22,23]. The object surface is probed with a very flexible cantilever, and the cantilever bending is optically registered by monitoring the position of the laser beam reflected from the cantilever (Figure 1a). During the scanning, interactions occur between atoms on the cantilever tip and atoms on the sample surface. To measure the mechanical properties, the cantilever performs single indentations over a defined area and obtains information about the stiffness of the material in the form of a load–displacement curve (Figure 1b). The resulting force curves (load–displacement curves) are subsequently processed by the software, which fits the curves to the selected mathematical model of tip-sample contact and calculates the Young's modulus value [26,27]. The Young's modulus indicates the material stiffness and is measured in Pascals (Pa). Tip radius and spring constant of the cantilever are of major importance for the resolution of images and quantitative evaluation of material properties [22] (Figure 1c,d). As the cantilever spring constant is an essential parameter for measurement of the object mechanics, one needs to have an approximate idea of the elastic modulus of the object under study (at least on the order of kPa, MPa or GPa) in order to select the appropriate cantilever in terms of its rigidity. The size of the AFM probe can also be regulated by attachment of differently sized tips to measure the mechanical properties of soft and hard biological materials, because the elastic modulus of biological objects varies significantly [25,28] (Figure 1e).

3. AFM methodology as applied to the ECM studies

In the ultrastructural AFM studies of the ECM, dried tissue sections on glass slides are commonly used [e.g. [13,21,31]. These are especially convenient since they can be used both for histological studies and AFM visualization. Histological staining does not interfere with AFM studies; moreover, it may be applied as a guide to select
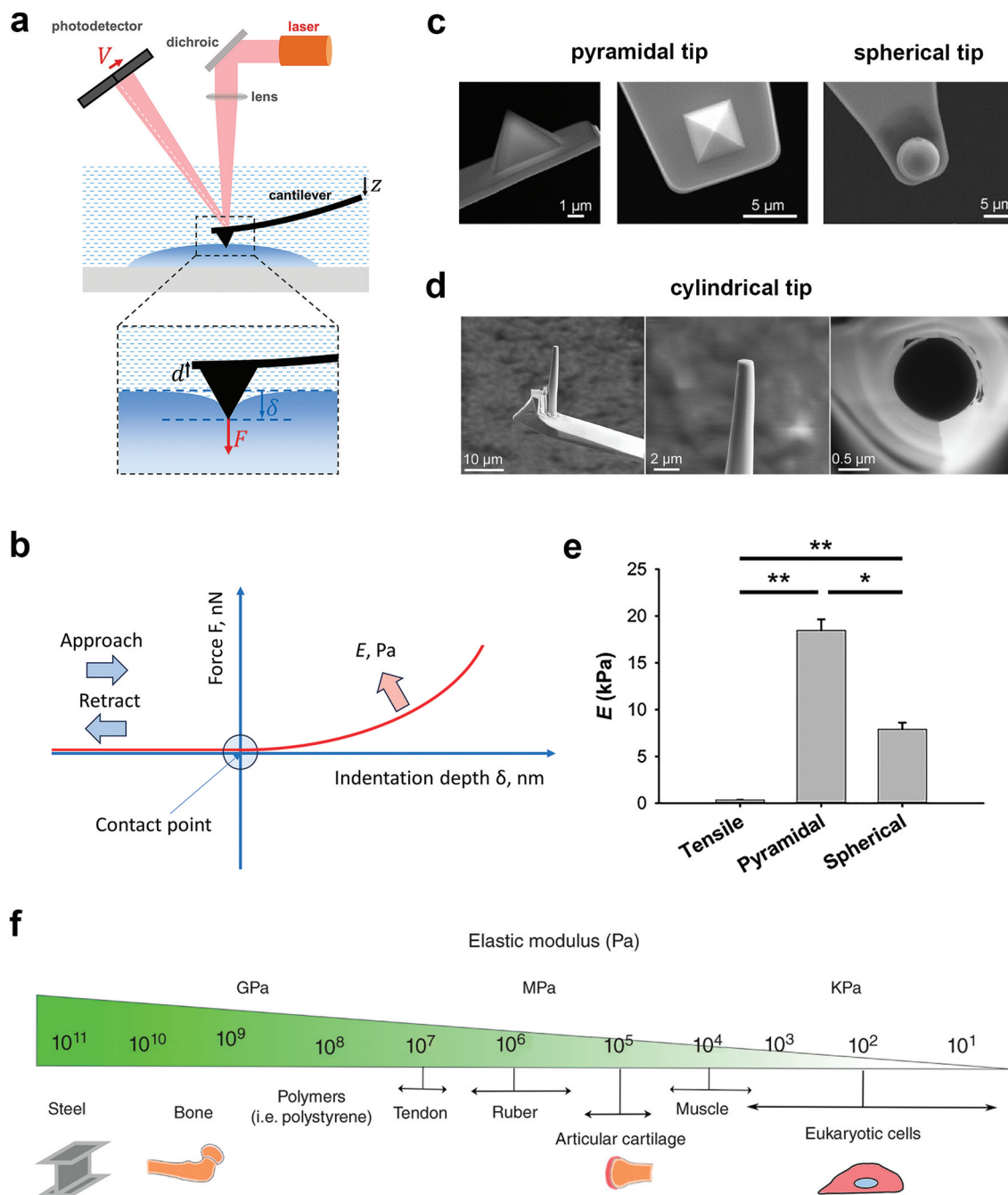
Figure 1. Measurement of material mechanical properties with AFM a – main elements of an AFM setup. A laser beam is focused on a cantilever, which is vertically displaced (z) with a piezoactuator. Cantilever deflection (d) occurs after sample indentation (δ) with the contact force (F). F is computed considering the cantilever stiffness and the voltage (V) produced in a photodetector by the displacement of the reflected beam, (reproduced by permission from [17], copyright [2016, WILEY]). b – force-distance (force vs. indentation) curve. c – scanning electron microscopy (SEM) images of a pyramidal tip, a spherical tip made of polystyrene bead (4.5 μm diameter) (reproduced by permission from [29], copyright [2016, WILEY]), d – SEM images of a microfabricated cylindrical flatended tip with cross-section of 1 μm2 in different views (reproduced under the terms of the Creative Commons Attribution License from [30], copyright [2012, Acerbi et al.]); e – Young's modulus of lung dECM at the unstretched state measured by macroscale tensile testing and by AFM measurements using pyramidal and spherical tips (indentation depth of 0.7 mm). Data are mean ± SE ($n = 9$). Statistical at $p < 0.05$ (*) and $p < 0.01$ (**) is indicated (reproduced by permission from [24], copyright [2019, Elsevier]). f – elastic modulus of various materials (reproduced by permission from [25], copyright [2014, WILEY]).

the region of interest (ROI) in the AFM studies. Since AFM scanning units are commonly installed on top of an inverted optical microscope, or are equipped with an upright optical microscope, the ROI are selected based on an optical view of the tissue section stained, e.g. for collagen. Thus, histology and AFM studies, as well as studies of tissue sections with other microscopic techniques, such as fluorescence microscopy or LSM, may become complementary for the most detailed structural description of the ECM [13,32]. AFM studies on air allow

for the highest resolution of the ECM ultrastructure, with the use of the corresponding AFM air probes with high spring constants.

Mechanical AFM studies require a different approach, since dried samples cannot provide adequate information on the ECM's real mechanical parameters. Thin tissue sections (10–50 μm) fabricated with a vibratome represent the most efficient type of samples for the precise AFM tip positioning using an inverted optical microscope [17]. The AFM imaging/ mechanical mapping is performed in the relevant media such as biological buffers. It is of note that the appropriate sample attachment plays a key role in such studies, so that the sample is not displaced by the moving AFM cantilever during force curve mapping in the liquid medium. The solution may be an attachment to glass slides pretreated with different agents, such as poly-L-lysine [17,27]. Another ECM sample type for biomechanical studies is the cell-derived ECM after removing cells [14,17]. As a rule, soft silicon nitride V-shaped AFM probes with very low spring constants (0.01–0.1 N/m) are used for mechanical studies of the ECM. Different computation models may be utilized to process the force-displacement data, depending on the AFM tip. The Hertz model for dull tips and microspheres and the Sneddon model for sharp tips are conventionally utilized. The effects of the sample thickness and viscoelasticity, as well as of the tip shape are frequently taken into account when analyzing the mechanical data [17].

4. Flicker-noise spectroscopy for the quantification of the ECM micro- and nanostructure

The ECM micro- and nanostructure is determined by the complex hierarchical arrangement of collagen fibrils, fibres and bundles of fibres. Various visualisation techniques, such as AFM, SEM, SGH, produce images with a 3D network of collagen structures which present mainly descriptive information. Using only descriptive data impedes the search for correlations between the structural characteristics and different factors potentially affecting them, facilitating the development of novel methods of quantification of 2D or 3D arrays of data obtained with visualization techniques. In AFM, the surface metrology parameters (ISO 25,178–2:2021), such as average roughness, rms roughness, skewness, kurtosis etc., are used most frequently to quantify the visualization data. However, the application of metrology parameters in the ECM studies is very limited, since these are integral parameters of surface heterogeneity, not accounting for the peculiar collagen packing, spatial periodicity, and sample history. The problem of the quantitative description of biological samples with a complex inner structure inspired the development of new computational approaches. For example, Talu et al. [33] applied fractal analysis to the images of the Bowman's membrane of the human cornea. For many ECM samples from various tissues, the flicker-noise spectroscopy (FNS) parameterization has appeared to be most instrumental, since it is capable of extracting the numerical information reflecting the ECM's intrinsic structure [31,32,34–37].

FNS represents a method of statistical physics, a general phenomenological approach to the analysis of complex nonlinear systems, which processes chaotic signals via ascribing informational significance to the temporal or spatial correlations in their sequences [38–41]. The fundamental concept of the FNS approach is based upon an assumption that the information about a complex system is contained in the sequences of irregularities of different types ('jumps', 'spikes', discontinuities in derivatives of different orders, etc.) observed in the sequence of values of a dynamic variable which describes the system. After removing the low-frequency component from the signal, the correlation links found in the chaotic component of the signal are described by a set of numerical parameters. These parameters may be used for further analysis as the system's quantitative characteristics.

In regard to AFM, the height profiles $h(x)$ are considered as dynamic variables. After separation of the low-frequency (resonant) component, the high-frequency chaotic component of a profile is analysed, and the autocorrelation function is considered for every profile. Two types of irregularities are analysed, 'jumps' (relatively moderate-height stepwise changes) and 'spikes' (bursts of a significant height, with dramatic height differences in a narrow x range). The details of the FNS computational approach to AFM images are described in [38,40]. Briefly, the correlation is assumed between the $h(x)$ and $h(x + \Delta)$, $\Delta > 0$, with the autocorrelation function $\psi(\Delta)$ for each profile

$$\psi(\Delta) = \langle 1muh(x)h(x+\Delta)\rangle_{L-\Delta} \quad (1)$$

where Δ is a spatial shift parameter, averaging within the L-Δ interval is defined by angular brackets.

The autocorrelation function $\psi(\Delta)$ is processed to produce the power spectrum $S(f_x)$

$$S(f_x) = \int_0^L \langle h(x)h(x+x_1)\rangle_{L-x_1} \cdot \cos(2\pi f_x x_1)dx_1 \quad (2)$$

where f_x is spatial frequency,

and the difference moment of second order $\Phi^{(2)}(\Delta)$

$$\Phi^{(2)}(\Delta) = \langle [h(x)h(x+\Delta)]^2\rangle_{L-\Delta} \quad (3)$$

Irregularities of different types have a different effect on $S(f_x)$ and $\Phi^{(2)}(\Delta)$, with only 'jumps' contributing to $\Phi^{(2)}(\Delta)$ and both 'jumps' and 'spikes' contributing to $S(f_x)$. Based on these two functions, $S(f_x)$ and $\Phi^{(2)}(\Delta)$,

several FNS parameters are defined using the comparison between the experimental and calculated data. The FNS approach was utilized in the analysis of a number of complex biological signals such as electrocardiograms [42], electroencephalograms [43,44], thermal lipid membrane fluctuations [45,46].

In 2015–2018, our research group had successfully applied the FNS parameterization approach in a number of studies on the ECM from various connective tissues [31,32,34–37]. We have shown that, of different FNS parameters, two basic parameters are most suitable for the ECM characterization: a 'stepwiseness factor' σ (nm), which reflects the jump-like irregularities of the studied AFM-profile, and a 'spikiness factor' $S(L_0^{-1})$ (nm^2 μm), which is a measure of spike-like irregularities, where L_0 is the length of correlation for the high-frequency irregularities at the nanoscale (for the details of obtaining these parameters, see [40].

In the study on the destruction of the collagen hierarchical structure in pelvic organ prolapse (POP) [31], a significant increase in both the σ and $S(L_0^{-1})$ parameters was noted for the POP-affected ECM, along with the increase in the peak-to-valley roughness. In terms of the FNS methodology, an increase in these two FNS parameters reflects the loss of order in the surface structure, which was in agreement with the visual observations of disordering in the collagen packing. The studies on the atherosclerotic plaques [32,34] showed that the values of the two FNS parameters correlated well with the morphological changes associated with the development of atherosclerosis. The FNS parameterization appeared most instrumental in the quantitative estimation of early damage to tissues by ionizing radiation during the radiation treatment of pelvic organs [36]. The ECM of the murine bladder, rectum and skin in the projection of the irradiation area were studied. In particular, the FNS parameters demonstrated a universal pattern of the dose-dependent morphology alteration in the ECM of the bladder, rectum and skin. At lower doses, the ECM underwent progressive disordering, while at higher doses, accumulation of non-collagenous material on top of collagen fibrils resulted in the surface smoothening and the decrease of σ and $S(L_0^{-1})$, correspondingly (Figure 2). In [35], the FNS approach was applied to quantify the ultrastructural morphological differences observed by AFM, associated with inflammation and urothelial carcinoma in the human bladder. It was shown that severe inflammation led to the collagen structure disordering (growth of the FNS parameters), while the presence of malignancy was related to the increased production of non-fibrous ECM components covering collagen fibrils with the decrease of both basic FNS parameters.

In contrast to surface metrology parameters, the FNS method, which includes a meticulous analysis of frequencies in the power spectra against the background of visual assessment of AFM images, provides filtered information reflecting the intrinsic structural features of the ECM. The revealed correlations in the chaotic height profiles appear sensitive to the ordered/disordered arrangement of collagen in the ECM and may be used as markers for the comparison of ECM in different conditions, e.g. in healthy and diseased tissue and potentially play a role in the computer-aided diagnostics. At the same time, the basic limitations of the FNS approach consist in the absence of direct reference to the structural characteristics of the collagen 3D network, such as fibril orientation, thickness of fibrils or collagen content.

Extracellular matrix is a multicomponent system with point-to-point variable mechanical properties, and its characterization with AFM could also benefit from an informatics-assisted AFM indentation method elaborated recently [47] for studying living cells, which are inhomogeneous membrane and fiber-based biological entities. The authors applied the Markov-chain Monte Carlo optimization to pick the fitting models for indentation force–displacement curves and AFM probe shape descriptors.

5. Overview of dECM application in research and therapy

In regenerative medicine, decellularized cell scaffolds may find applications for wound healing and even whole-organ transplantation (Figure 3). The regenerative potential of tissues varies significantly. While bone can heal itself (if the lesion size does not exceed 2.5 cm), cartilage has low regeneration ability because of low chondrocyte cell density and lack of blood vessels [49]. Currently, organ transplantation is the only treatment at the late stages of some severe diseases such as pulmonary fibrosis, chronic obstructive pulmonary disease, alpha-1-antitrypsin deficiency, pulmonary arterial hypertension and others [50]. The shortage of donor organs for transplantation is the major obstacle for the treatment, so their replacement with bioartificial organs engineered using repopulated decellularized ECM scaffolds could be a desirable alternative [51]. Cell removal from allogeneic tissue results in a close to native and nonimmunogenic framework that can be then repopulated with autologous cells. An interesting observation here is that the properties of seeded cells can be modified in vitro through dECM signalling. Thus, expanding bone marrow-derived MSCs (BMCs) from older organisms on dECM produced by BMCs of younger organisms rejuvenated key properties of the aged BMC cells [52]. Moreover, dECM-based tissue engineering potentially allows obtaining highly compatible transplantation organs, grown in vitro from the patient's own cell
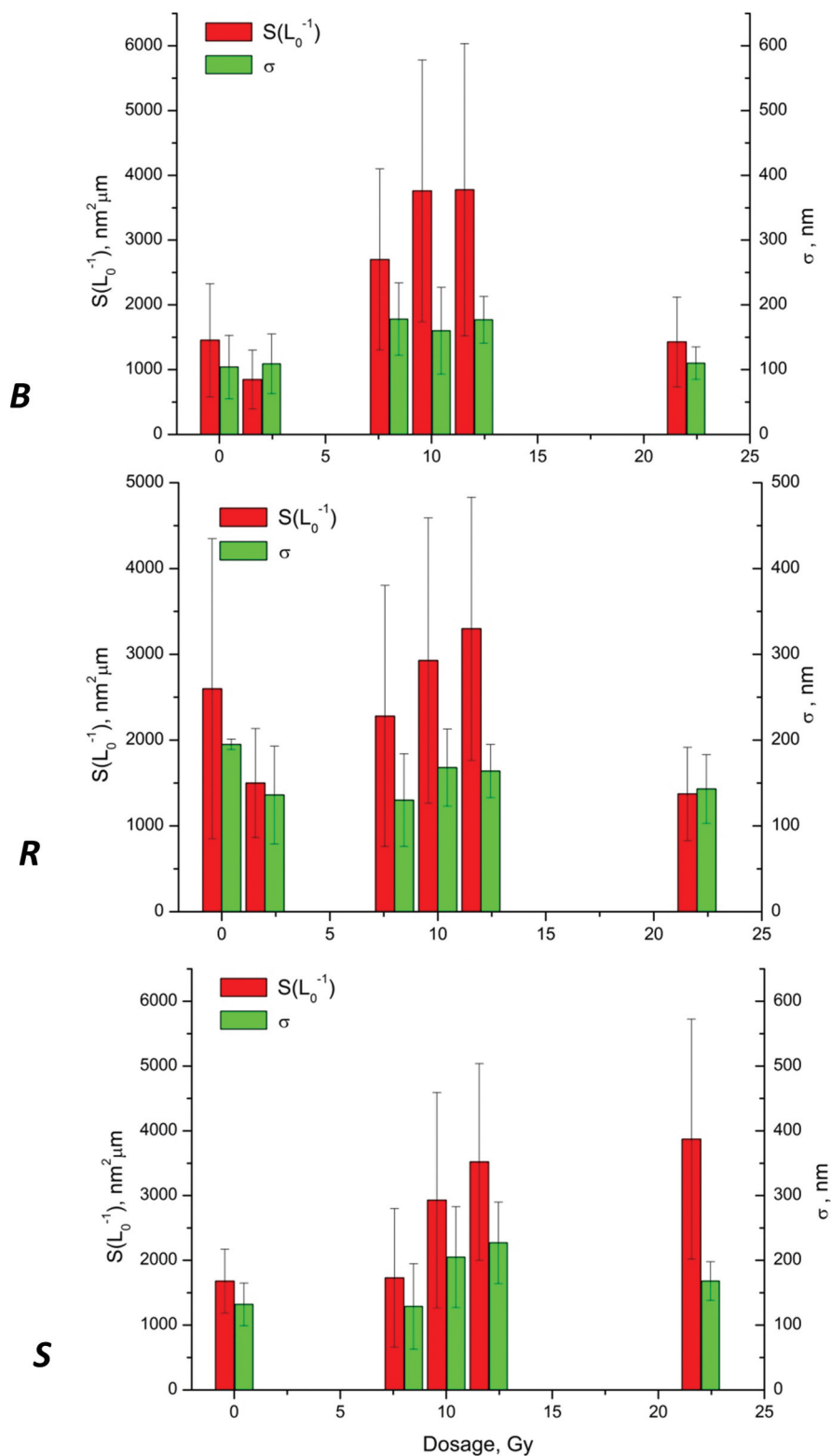
Figure 2. FNS parameterization of the AFM images of the ECM of the murine bladder (B), rectum (R) and skin (S) after irradiation with different doses. The sizes of AFM images are $6 \times 6\,\mu m$. Reproduced by permission from [36], copyright [2018, Oxford University Press]).

and tissue samples. It is assumed that such scaffolds containing biochemical and mechanical stimuli will support cell proliferation and differentiation with better grafting and tissue regeneration outcomes.

There are two principal sources of decellularized matrices for tissue engineering: tissues/organs isolated from various organisms and ECM derived from cells cultured in vitro [53]. Decellularized whole organs can be used for transplantation, as they retain the general organ structure [15]. A major challenge in converting decellularized whole solid organs to transplantable grafts is
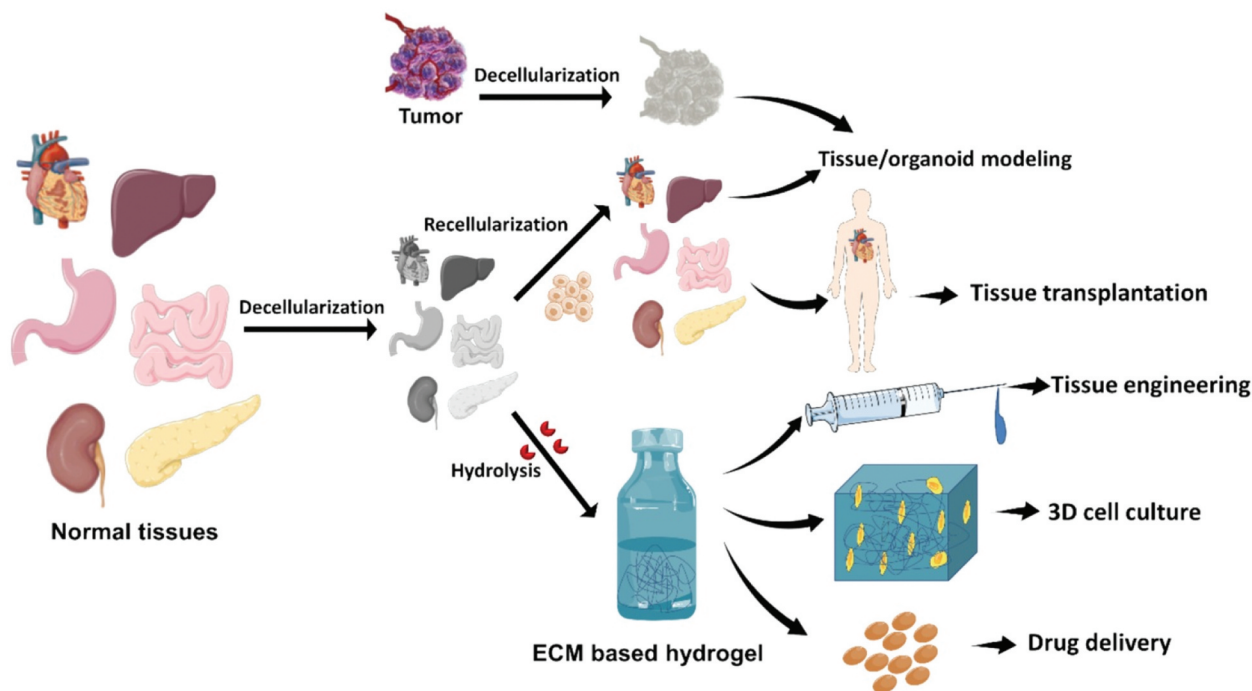
Figure 3. Whole tissue/organ decellularization and applications of dECM-based materials (reproduced by permission from [48], copyright [2019, Elsevier]).

a vascular reconstruction, and various methods of reendothelialization enhancement have been tested for liver, kidney, lung and heart [54]. As an alternative to applying a whole decellularized tissue or organ scaffold, decellularized ECM can be powdered and then used to obtain printable or injectable hydrogels, inks or bioinks with tuneable properties [55,56]. dECM hydrogels can be used as culture substrates, and as injectable materials to fill and repair irregularly shaped tissue defects [57].

In vitro differentiation of pluripotent stem cells is a potential way to overcome the shortage of transplantable materials. As a source material for producing in vitro engineered implants, dECM of adipose tissue seeded with autologous adipose stem cells and treated with corresponding growth factors to induce differentiation can be used, considering the relatively high availability of adipose tissue wastes from liposuction and abdominoplasty [58]. Mesenchymal stem cells (MSCs) isolated from various tissues can be expanded in vitro and used for therapeutic applications, including direct MSC transplantation into the injury site or the use of MSC secreted products [59]. Decellularized ECM produced by MSC has been tested as culture substrates for in vitro MSC expansion or differentiation of reseeded MSC into desired lineage [59]. MSC dECM can be obtained in large quantities from in vitro cultured iPSC-derived MSCs or a stable MSC cell line created from MSCs isolated from the human placenta transduced with human telomerase reverse transcriptase (hTERT) [52]. The chemistry of the underlying substrate had been

reported not to influence ECM deposition by MSC and its activity, implying that a wide variety of substrates is suitable for dECM production [60]. However, other studies demonstrated that appropriate surface properties are crucial for self-assembly of some ECM components (e.g. fibrinogen proteins) and initiation of ECM self-organization [61].

When dECM is obtained from in vitro cell cultures, the composition and properties of dECM can be tuned by changing the cultivation conditions or genetically engineering the ECM producing cells. For instance, the addition of ascorbate to culture medium can result in increased collagen I content [62]. An ECM with enhanced angiogenic potential was produced by cultivating a vascular endothelial growth factor alpha (VEGF)-over-expressing immortalized human mesenchymal stromal cell (hMSC) line [63]. VEGF-over-expressing hMSC deposited a VEGF-enriched ECM, which, after decellularization, supported a much deeper penetration of host vasculature toward the centre of the dECM-based implants [63]. For highly mechanosensitive tissues such as cartilage, the compressive loading on a corresponding dECM-derived scaffold during chondrocyte growth in vitro also modulates the synthesis of ECM molecules and improves the newly-synthesized fibre alignment and the Young's modulus of the engineered construct [64].

Decellularization technique offers various possibilities for ex vivo research in fundamental science and personalized medicine, allowing disease modelling and drug

screening. The behaviour of cells in DECM obtained from healthy and diseased tissues of a particular patient can be compared to study the role of ECM properties in disease progression [65]. Decellularized tissues can be modified in vitro, for example, by collagen glycation, to study the changes in ECM topography and mechanical properties under modelled disease conditions [66]. Extracellular matrix hydrogels derived from decellularized tissues can support organoid cultures from healthy [67,68] and tumour organoids [69] to develop more representative human organ models. The decellularized tumour ECM was employed to create a tumour-specific hydrogel that supported patient-derived tumour organoids, which provides a new avenue for personalized medicine applications [69].

6. The composition of the extracellular matrix

The major structural components of ECM are mesh-forming fibrous proteins (collagens, elastins), glycoproteins (laminin, fibronectin, and others), proteoglycans, and glycosaminoglycans although the composition of dECM depends on tissue type and

tissue location (Figure 4) [1]. Collagens are a large family of related proteins, with different collagen species predominating in ECM of distinct anatomic locations such as type I collagen in lung [70], type II in cartilage and type IV collagen in basement membranes [71], which are specialized ECM sheets that form the foundation of all complex tissues. Collagens assemble into a variety of supramolecular structures, such as fibrils, filaments, or networks [63]. Individual collagen fibrils demonstrate characteristic periodic D-spacing [72] (Figure 5a,b). Variations in collagen thickness and D-spacing can be observed in distinct locations where collagen fibrils consist of several collagen types [75]. Collagen fibres are structurally and mechanically anisotropic, and thus the radial compressive stiffness of the collagen fibres measured by AFM nanoindentation is different from their axial tensile stiffness [76]. Moreover, changes in the radial compressive stiffness of individual collagen fibres do not necessarily translate to the axial elasticity changes [76].

The high capacity of some soft tissues to undergo large elastic strains is partly explained by reorganization of collagen fibres within the ECM [75]. At small strains, the fibres are randomly distributed, resulting in low
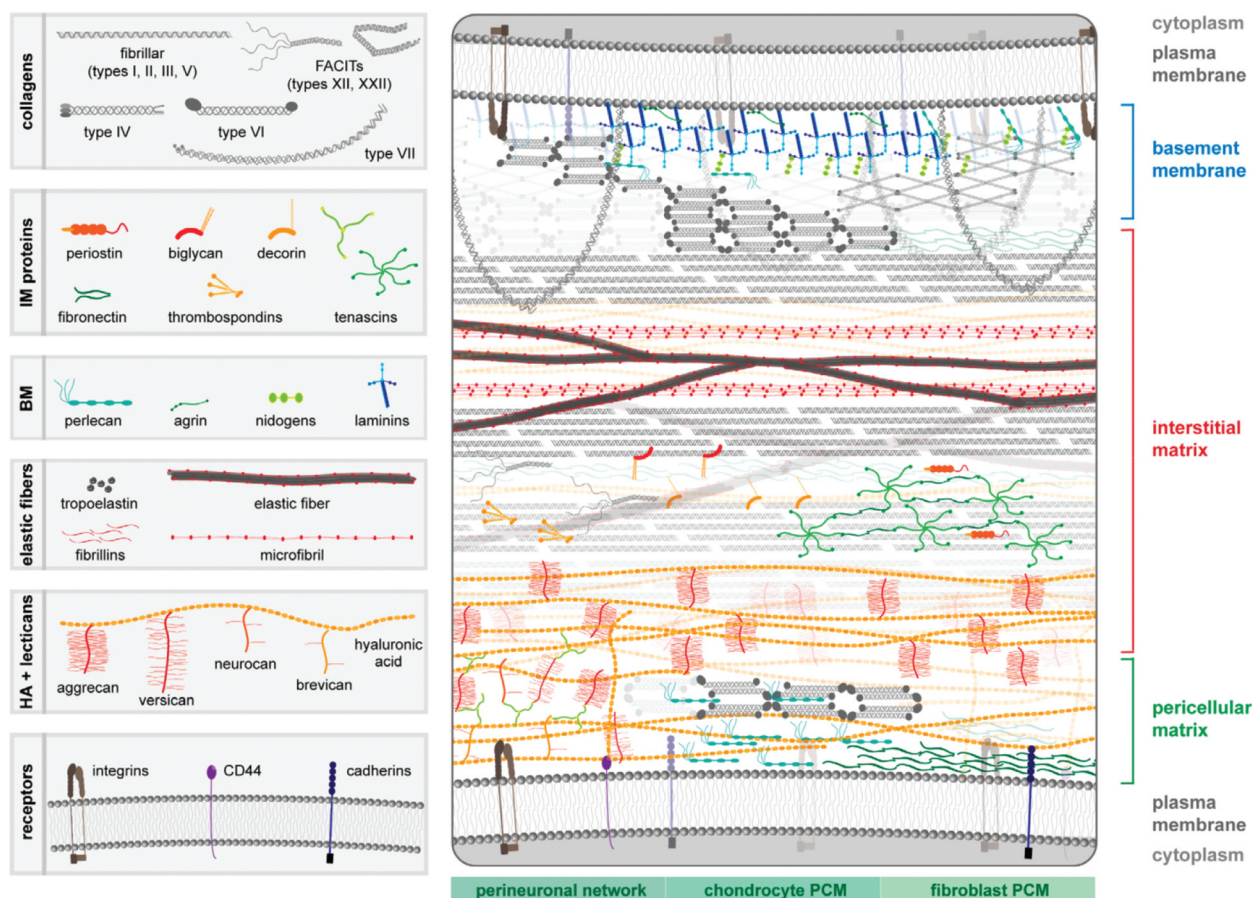

Figure 4. General view of ECM and its major components (not to scale). Three regions of ECM are shown: the basement membrane (BM), interstitial matrix (IM) and pericellular matrix (PCM). The upper cell is an endothelial or epidermal cell separated from the interstitial matrix (IM) by the basement membrane (BM). The BM is connected with the IM through type VI collagen and/or type VII collagen anchoring fibrils. The pericellular matrix (PCM) encompasses the bottom cell (reproduced by permission from [1], copyright [2021, Elsevier]).
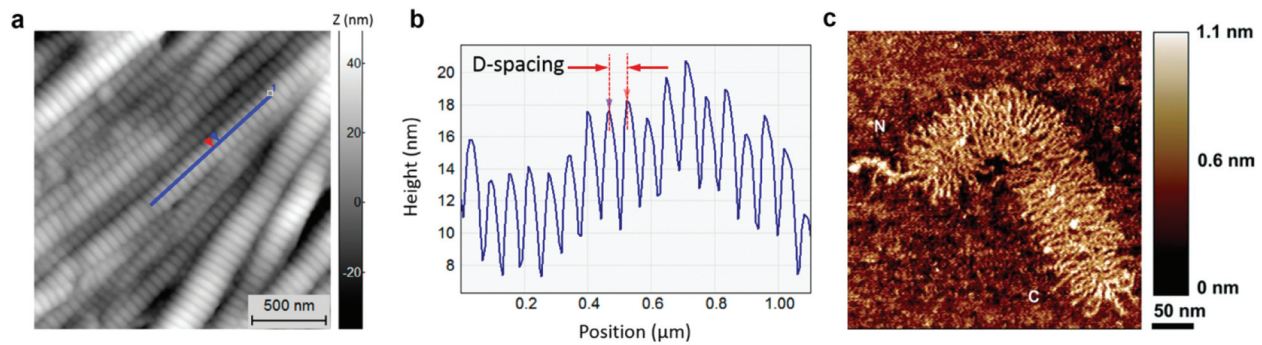
Figure 5. Major ECM components visualized by AFM. a – topography images of collagen fibrils in the annulus fibrosus of intervertebral disc; b – height profile of the fibril shown in a with the peak-to-peak distance corresponding to collagen D-spacing (reproduced from [73] under the terms of the Creative Commons CC BY license copyright [2020, Cauble et al.]). c – AFM height images of an individual isolated fetal epiphyseal aggrecan monomer with N- and C-terminal regions of the core protein designated (reproduced by permission from [74], copyright [2003, Elsevier]).

tissue stiffness, primarily on the order of kilopascal. When large strains are applied, the collagen fibres align and form a stiff network, with tissue stiffness increasing up to that of collagen fibrils, which lies within the megapascals (MPa) and gigapascals (GPa) ranges in hydrated and dehydrated states, respectively [75].

The largest structures in the ECM are elastic fibres that provide the elasticity of tissues such as the large arteries, lung, and skin. They consist of two components: elastin protein (a cross-linked insoluble polymer of a soluble tropoelastin) and 10–15-nm '"microfibrils"' (with fibrillins as the main component). A number of proteins are associated with microfibrils or elastin such as the microfibril associated glycoproteins (MAGPs), fibulins, EMILIN-1 and others [77].

A network of collagen fibrils and elastic fibres is embedded in a hydrated gel made of proteoglycans and glycosaminoglycans (GAG) (Figure 5c). Glycosaminoglycans are negatively charged polysaccharides which are divided into five families: chondroitin sulphate, dermatan sulphate, heparan sulphate, keratan sulphate, and hyaluronan. Polymeric GAGs can remain as free polysaccharides or can be covalently bound to proteins to produce proteoglycans [78], such as aggrecan, the major proteoglycan in the cartilaginous tissue ECM [74]. The biological activity of GAGs significantly depends on their negative charge, which in all GAGs, except for hyaluronan, is associated with the presence of sulphated residues [79]. The negative charge of hyaluronan results from the presence of glucuronic acid, and hyaluronan is the only GAG that does not bind proteins to form proteoglycans but interacts with other ECM components as it is [79]. In cartilage, the GAG chains of aggrecan are the major determinant of the cartilage compressive stiffness, which was supported by direct measurement of intermolecular repulsion forces between negatively charged GAG by AFM [80]. The core protein of aggrecan has different

GAG substitutions in various biological species and GAG chain length and sulphate ester substitution of aggrecan vary as a function of age and disease, which was also confirmed by direct AFM imaging [74]. Decellularization can result in disproportionate losses of specific GAGs and changes in GAG disaccharide composition affecting the dECM binding of matrix-associated growth factors, as it was demonstrated in human lung dECM [81].

In humans, ECM in some tissues (bones, teeth, and the hypertrophic zones of growth plate cartilage) contain inorganic components appearing due to mineralization process. Calcification of vascular tissue ECM also occur as a complication of atherosclerosis, and diabetes, and during aging, and crystals appear to form preferentially on protein templates [82].

AFM contributed to characterization of ECM components and their self-organization into a complex supramolecular structures. Using shear modulation force microscopy, an AFM-based technique, it was found that fibronectin protein spontaneously self-assemble into fibrils on high fixed-charge density surfaces, which explained the long observation that fibronectin fibrils could form only on cell surfaces or lipid bilayer surfaces mimicking the plasma membrane [61]. The self-assembly of elastin to nanofibrils, then to fibrils and eventually to fibres from elastin suspensions was also recently studied using AFM [83].

A different organization of ECM in various organs was revealed by morphological examinations of dehydrated [84] or cryo-sectioned [13] tissues with AFM operating in the tapping mode. In human articular cartilage, the ECM was primarily composed of thick and thin type II collagen fibrils (identifiable by their characteristic 67 nm periodic structure) embedded within a proteoglycan (aggrecan) matrix; in the ferret left ventricle epicardium, collagen fibrils were arranged into sheets and oriented along the direction of the contractile force; in human skin, 'basket-weave' bundles of fibrillar collagen were visible; in the murine lung,
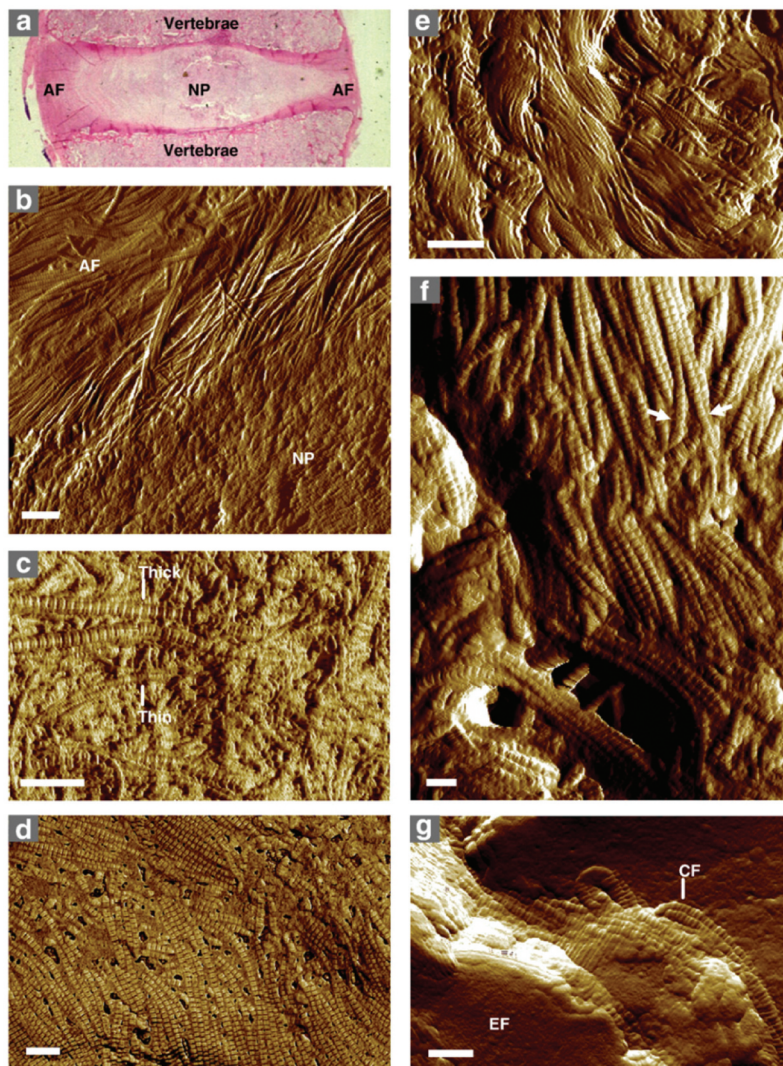
Figure 6. Distinct ECM organization in different locations visualized by AFM. a – haematoxylin and eosin staining of intervertebral disc demonstrates the presence of two distinct regions, an inner, cartilage-like nucleus pulposus (NP), and an outer, tendon-like, type I collagen-rich annulus fibrosus (AF). b – the same regions visualized by AFM in the bovine intervertebral disc. c – human articular cartilage with thick and thin collagen II fibrils embedded in an aggrecan matrix. d – AFM phase images of the ferret left ventricle epicardium with collagen fibrils oriented in the direction of the contractile force. e – In amplitude images of human skin cryo-sections with characteristic intercalated 'basket-weave' of fibrillar collagen bundles. f – individual collagen fibrils (arrows) form laterally associated bundles in the murine. g – ovine aorta elastic lamellae with elastin-rich fibres (EF) and an inter-lamellar space with collagen fibrils (CF). Scale bars are1 µm (b and e), 500 nm (c and d) and 200 nm (f and g)(Reproduced by permission from [13], copyright [2010, Elsevier]).

individual fibrils of collagen formed laterally associated bundles that branched and connected with each other; while in the ovine aorta, granular elastin-rich regions intermitted with collagen fibrils [13] (Figure 6).

ECM compositional differences are expressed in significantly different biomechanical properties of the ECM, measured by AFM [85]. As the diameter of individual collagen fibres (0.5–1.5 µm) can be comparable to the size of the contact area with an AFM tip, the estimated value of local Young's modulus depends on a variable contribution of the stiff fibers and soft proteoglycans between them [24]. Both dECM stiffens and composition influences cell differentiation [86] and cell stiffness [87]. The geometry and mechanical properties of elastin and collagen fibres change during aging or disease [88–90].

7. Decellularized ECM: sources and methods

We will only briefly describe decellularization methods here because a number of excellent reviews on the topic were published recently [91,92]. The decellularization can be performed by physical, enzymatic, and chemical methods and their combinations (Figure 7). Physical methods include freeze/thaw cycles, hydrostatic pressure, supercritical carbon dioxide or electric shock, electroporation, and ultrasound [92].

Chemical methods include tissue treatment with acids (for instance, peracetic acid and acetic acid), bases (such as sodium hydroxide) or detergents. As acids and bases are rather harsh agents, which can damage dECM structure and composition, chemical decellularization is usually performed with nonionic,
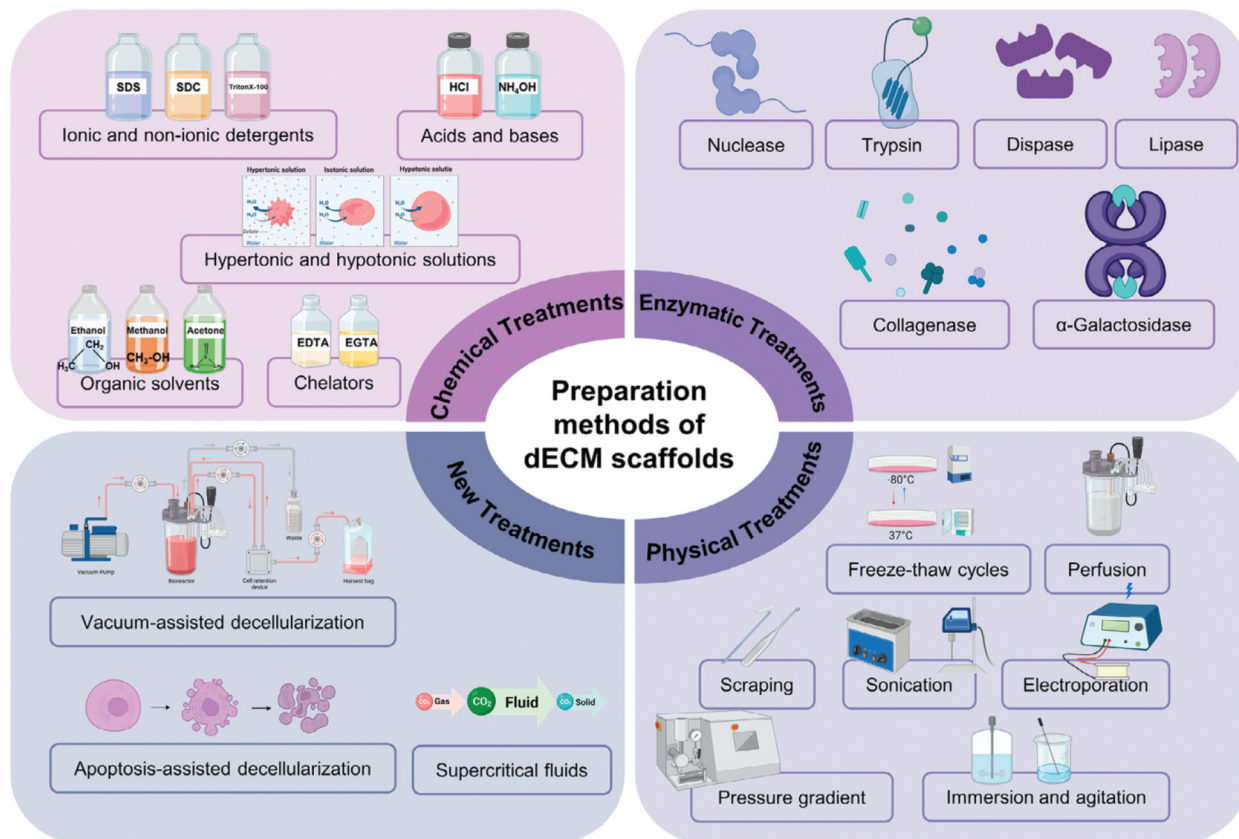
Figure 7. Classification of main decellularization methods (reproduced from [15] under the terms of the Creative Commons CC BY license copyright [2024, Liu et al.]).

ionic, and zwitterionic detergents. The detergents disrupt the cellular membranes but can denaturate proteins or disturb protein–protein interactions. Ionic detergents (sodium dodecyl sulphate (SDS)) were reported to be more detrimental to protein structure than zwitterionic detergents such as 3-([3-cholamidopropyl] dimethylammonio)-1-propanesulfonate (CHAPS)) and ionionic detergents such as Triton X-100 [49]. However, although Triton X-100 is regarded as a weaker detergent than SDS, it caused disruption of the collagen structure of rat tail tendon, while SDS in the same concentration did not cause significant collagen denaturation [93]. No evidence of fibronectin or collagen denaturation after repeated SDS treatments of caprine pancreas was found [94]. This underlines the importance of a careful choice of decellularization protocol corresponding to a specific tissue type and full characterization of the resulting tissue dECM.

The toxicity of surfactants could be a major problem. Although SDS and Triton X-100 (alone or in combination) are often used to obtain cell-free ECM scaffolds, in some studies fibroblasts did not colonize the scaffolds prepared with the use of SDS or Triton X-100 [95]. However, when surfactant-treated decellularized matrix was solubilized to bioink to be used in bioprinting, no cytotoxicity to fibroblasts was reported [96].

Chondrocytes successfully colonized dECM substrates prepared with SDS [97] or Triton X-100 [98]. Recently, sodium deoxycholate was reported as being a better detergent for decellularization of porcine and murine (mice and rat) lung, heart, kidney, and bladder glass-attached thin tissue slices than CHAPS, Triton X-100, ammonia hydroxide and SDS, allowing efficient DNA removal with sufficient elastin retention [99]. As the glass-attached thin tissue slices were used for decellularization, this method allows AFM measurements of the mechanical properties on the same tissue section before and after decellularization.

Biological methods include the treatment of tissues with proteases (mainly trypsin) and nucleases (DNase and RNase). Chelating agents such as ethylenediaminetetraacetic acid (EDTA) can be also applied to detach cells without lysing them and to improve decellularization [100]. A novel approach to ECM decellularization was proposed recently, in which in vitro cultured cells were modified by insertion of a triggered apoptotic genetic construct that allowed to obtain dECM by inducing cell apoptosis, followed by dECM washing with PBS to remove the cell debris [63]. The dECM-based grafts obtained by this method were superior in supporting bone regeneration as compared to the dECM-based grafts decellularized by the freeze–thaw technique, likely because of better preservation of the ECM composition [63].

Alternatively, dECM can be obtained by inducing cell apoptosis with chemical inductors such as rotenone [101] or camptothecin [102]. Allogenic and xenogeneic scaffolds, made by apoptosis-assisted decellularization are regarded as less immunogenic and thus having lower risk of rejection after transplantation than scaffolds decellularized by conventional methods [103].

As the composition of ECM is tissue-type specific, decellularization protocols should be tailored for different tissues [49]. The point is to achieve complete decellularization without significantly affecting ECM structure and composition. During decellularization, it is important to efficiently degrade and remove nucleic acids from the donor material to mitigate host immune reaction after transplantation [104]. The quality of the decellularization procedure is evaluated by comparing nucleic acid contents before and after the procedure and determining the presence of essential ECM constituents by immunohistochemistry (IHC), histologic staining, ELISA, and mass spectrometry [105].

According to the origin of ECM, dECM scaffolds are classified as autologous dECM, allogeneic dECM (different individuals of the same species) and xenogeneic dECM (different species). However, architectural and compositional differences, and immunogenicity problems in case of incomplete decellularization may take place if allogeneic/xenogeneic dECM are used for tissue engineering purposes [106], although the immune response depends on the tissue type and even on the particular lesion location [107]. It was reported that the decellularization method impacts the host macrophage behavior and thus the outcome of the dECM-based material implantation [108]. In order to obtain a whole decellularized organ, an organ is perfused with decellularizing agents through the natural tubular pathways such as blood vessels, liver bile ducts, lung airways, and kidneys ureters [92].

Decellularized ECM is sometimes pulverized to powder to facilitate the decellularization process and then the powder is moulded to a porous cell scaffold of designed an antomically relevant shape [109]. To avoid scaffold contraction after cell seeding various approaches are used in order to increase the scaffold compressive modulus such as chemical cross-linking, reinforcing with synthetic polymers, and UV and dehydrothermal treatment, or using high dECM concentrations together with pore alignment via unidirectional freezing [109].

AFM has also been used to assess the dECM architecture and mechanics in order to find an optimal decellularization protocol for a given tissue [28,95]. AFM analysis confirmed better performance of cold EDTA than Triton X-100 as a decellularization agent for cultures of hTERT-immortalized myometrial smooth muscle cells and U2OS osteosarcoma cells by demonstrating that the Triton X-100-treated specimen was contaminated with the debris of disrupted cells, while the surface of EDTA-treated dECM was free from cell-derived contaminants (Figure 8) [100]. The use of SDS for porcine heart decellularization allowed better preservation of the ECM microarchitecture than Triton X-100 or trypsin treatment [110]. Higher proliferation of rat myocardial fibroblasts and better alignment of neonatal rat cardiomyocytes in the scaffolds made of SDS-treated dECM were observed in seeding experiments, which was probably associated with significantly higher surface roughness of the SDS-treated tissue, registered by AFM (Figure 9) [110]. Thus, the characterization of scaffold nanoarchitectural and nanomechanical traits with AFM could prove useful to explain the results on cell proliferation in dECM scaffolds produced with different decellularization protocols.

8. The importance of dECM mechanical properties characterization

In addition to chemical signals, reproducing the mechanical properties of cell microenvironment is of crucial importance. Cells sense and respond to the mechanical stimuli, such as substrate rigidity, viscosity, and mechanical strain [111–114]. Many diseases are associated with changes in cellular mechanotransduction (Table 1) [115]. The characteristic cell behaviour, including cell migration [111], movements [116], proliferation [117], and differentiation [118] depends on substrate mechanical properties. For instance, embryo-derived cardiomyocytes beat best on a matrix with heart-like elasticity, while rigid substrates mechanically similar to a fibrotic scar stop their beating [116]. The cell response to the substrate stiffness is cell type-specific [117], which is associated with variability in ECM stiffness in different locations in vivo [119,120] (Figure 10a). Moreover, the ECM stiffness changes as a result of disease such as cancer [121] or fibrosis [122] (Figure 10b), and the diseased tissue can become either softer (in arthritis or emphysema) or stiffer (in fibrosis, sclerosis, or cancer) than the healthy one [28]. The changes in ECM mechanical properties can contribute to malignant transformation of cells [123–125]. Oppositely, mechanical cues from softer dECM of healthy cells can suppress proliferation of cancer cells [126]. Matrix stiffness was also reported to be related to chemoresistance of tumours, although the complete mechanisms await elucidation [127]. The ECM structure also influences angiogenesis, and thus the wound healing process [115]. The interplay between the stiffness of the cell and its microenvironment determines the cell invasion behaviour and thus is important for the clinical outcome of various
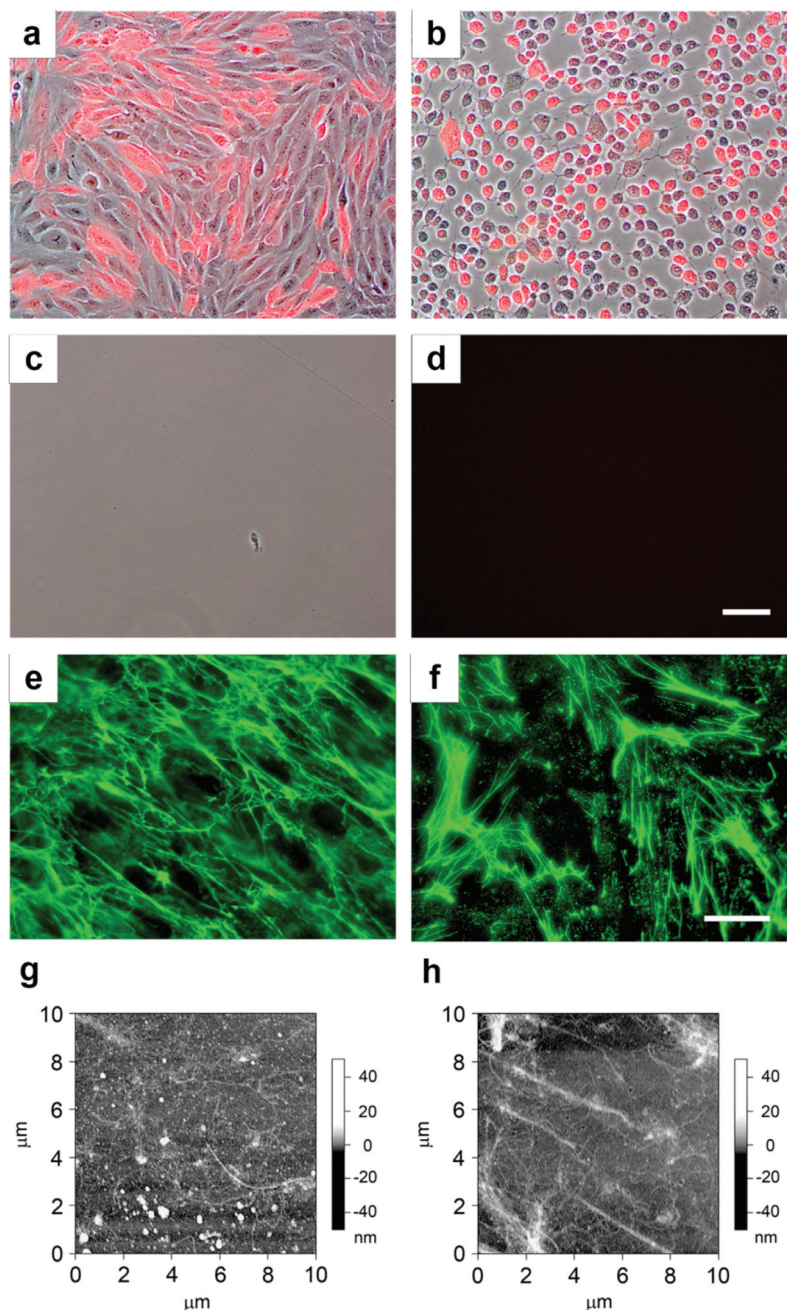
Figure 8. Use of AFM along with other methods for assessment of the decellularization efficiency and the quality of the scaffold obtained from decellularized ECM deposited by cultured hTERT-myometrial smooth muscle cells. Superimposed fluorescent and DIC images of (a) hTERT-myomSMCs expressing mCherry which were grown for 3 days on uncoated glass coverslips and (b) rounded mCherry-expressing hTERT-myomSMCs after treatment with cold EDTA. Culture plate from which the cells treated with cold EDTA were washed with PBS, visualized by DIC (c) and fluorescent imaging (d). Immunofluorescent images of ECM fibronectin in hTERT-myomSMC culture prior to (e) and after (f) decellularization with cold EDTA. Scale bars, (a-d) 100 μm; (e and f) 20 μm. AFM images of ECM decellularized with (g) triton-X-100 and (h) cold-EDTA. (g-h) AFM gray scale bars show the z-axis dimensions (reproduced by permission from [100], copyright [2014, Elsevier]).

matrices application for therapeutic purposes [87]. The donor age does not significantly influence dECM local stiffness, as it was shown by AFM studies in mice lungs, while a diseased state such as fibrosis has a very large impact [122]. Decellularized ECM scaffolds obtained from diseased tissues can be applied to investigate the role the matrix stiffness plays in disease progression and for preclinical drug screening [128], necessitating thorough characterization of dECM mechanical properties.

AFM can provide valuable information on dECM scaffold stiffness and architecture. While micromechanical and nanomechanical dECM properties can be registered using CellScale MicroSquisher tension-compression test system [129] or in situ nanomechanical indentation test system [130], AFM allows simultaneous registration of mechanical and morphological properties. According to AFM analysis, the dECM scaffolds obtained from fibrotic lungs displayed regions with stiffness comparable to normal tissue
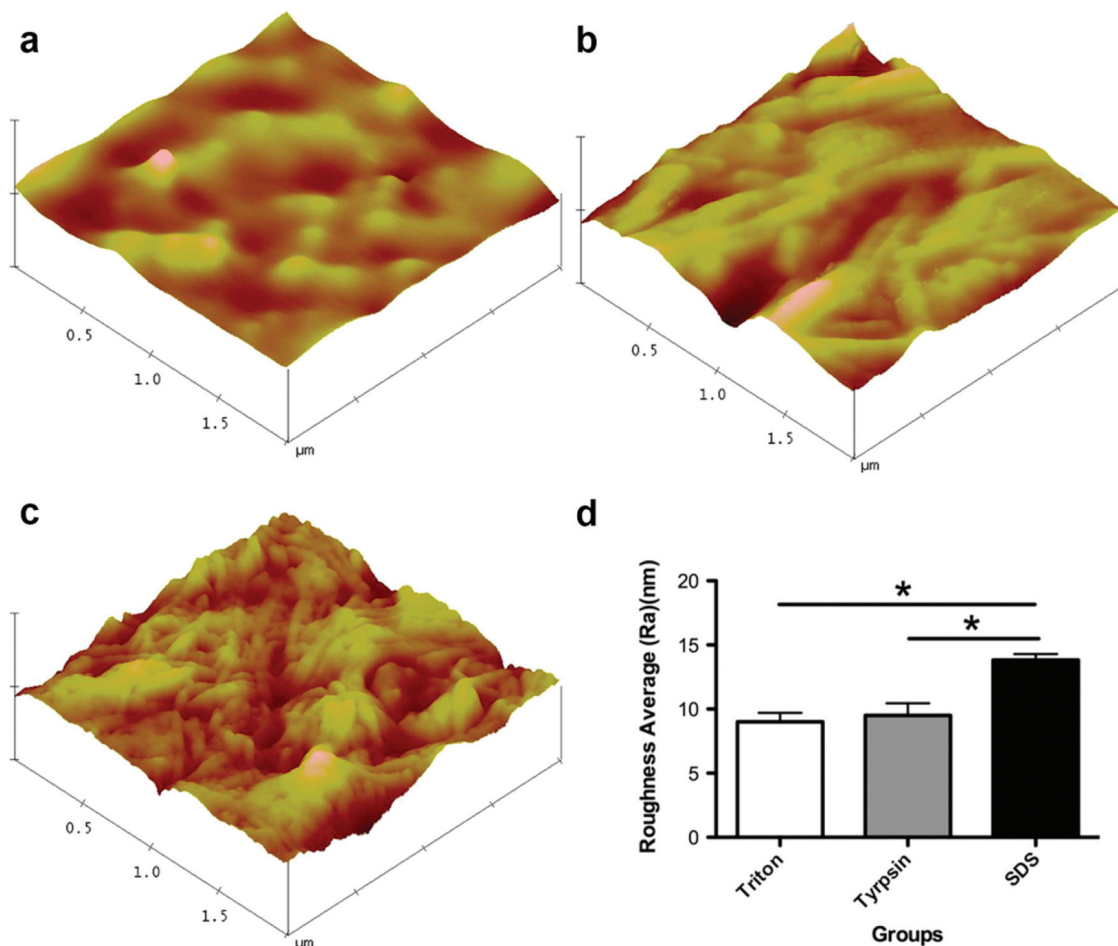
Figure 9. AFM images of the surface topography of the porcine heart tissue after decellularization with triton X-100 (a), trypsin (b) or SDS (c). Each AFM image size is 2.0 μm × 2.0 μm. d -The tissue treated with SDS is rougher (has a higher roughness average (ra) value) than the other two treatments. Data are mean ± SD with statistically significant difference indicated with * (reproduced by permission from [110], copyright [2016, Springer Nature Customer Service Centre GmbH).

and regions with much higher stiffness, and promoted transforming growth factor-β (TGF-β) – independent fibroblast differentiation to myofibroblasts [70].

AFM analysis revealed that the topography and stiffness of dECM derived from neoplastic tissues are different from those from normal tissues, with neoplastic tissues dECM being stiffer and less organized than dECM from the healthy tissue [65,121] (Figure 11). The specific scaffold traits resulted in preferential growth of organoids developed from colorectal cancer peritoneal metastases on scaffolds from neoplastic peritoneum in comparison to normal scaffolds [65]. When the Young moduli of dECM obtained from healthy and neoplastic tissues of the same patient were compared with AFM, a significantly increased neoplastic dECM stiffness was found, which was associated with disorganized collagen accumulation [121].

The mechanistic explanation of intra-tissue variability in the dECM stiffness is difficult. It has been related to differences in the dECM composition, particularly, in the collagen and elastin contents [119,120]. When AFM stiffness maps were registered in non-fixed slices of decellularized healthy heart

tissue immunostained for elastin and collagen, the elastin-rich sites around the vessels were found to be about two times stiffer (E = 74.5 ± 8.7 kPa) than collagen-rich sites in the myocardium (E = 30.2 ± 2.8 kPa) and pericardium (E = 32.9 ± 4.3 kPa) [120]. The E in collagen-rich regions of decellularized heart tissue from wild-type mice was about 30 kPa and increased three-fold in infarcted heart tissue, which was associated with a dramatic increase in collagen deposition, but could also be related to ECM cross-linking and changes in fibre structure [120].

Scaffold preparation can also influence the registered stiffness. In dECM derived from cultured human pulmonary fibroblasts, the matrix stiffness depended on the cross-linking of extracellular matrix molecules with glutaraldehyde rather than collagen I content [62]. However, specimen treatment with glutaraldehyde not necessarily changes the ECM mechanical properties, as it was demonstrated in inner limiting membrane (an ocular basement membrane that separates the retina from the vitreous humour) [85]. The authors supposed that it was due either to already maximal cross-linking of all components or

Table 1. A partial list of diseases with aetiology or clinical presentation resulting from abnormal mechanotransduction (reproduced by permission from [115], copyright [2009, Taylor & Francis Ltd]). In the right column the letters indicate whether the mechanical basis of the disease results from changes in cell mechanics (C), in tissue structure (T) or mechanochemical conversion (M). '?' – indicates that deregulation of mechanical conversion is possible but needs to be demonstrated.

Cardiology	Angina (vasospasm)	C T
	Atherosclerosis	T M
	Atrial fibrillation	M
	Heart failure	C T M?
	Hypertension	C T M?
	Intimal hyperplasia	C T M?
	Valve disease	T
Dermatology	Scleroderma	T
Gastroenterology	Achalasia	C
	Irritable bowel syndrome	C M?
	Volvulus	C T
Nephrology	Diabetic nephropathy	C T M?
	Glomerulosclerosis	C T M?
Neurology	Cerebral edema	T
	Facial tics	C
	Hydrocephalus	T C?
	Migraine	C M?
	Stroke	C T
	Stuttering	C
Oncology	Cancer	C T M?
	Metastasis	C
Opthalmology	Glaucoma	C T M?
Orthopedics	Ankylosing spondylitis	C T
	Carpal tunnel syndrome	C T
	Chronic back pain	C T
	Dupytren's contracture	C T
	Osteoporosis	T M
	Osteoarthritis	T
	Rheumatoid arthritis	T
Pediatrics	Collagenopathies	T
	Congenital deafness	C T M
	Mucopolysaccharidoses	T
	Musculodystrophies	C T M
	Osteochondroplasias	C T
	Polycystic kidney disease	T M
	Pulmonary hypertension of newborn	C T M?
Pulmonary medicine	ARDS	C T M?
	Asthma	C T M?
	Emphysema	T
	Pulmonary fibrosis	T
	Pulmonary hypertension	C T M?
	Ventilator injury	C M
Reproductive medicine	Pre-eclampsia	C T M?
	Sexual dysfunction (male & female)	C M?
Urology	Urinary frequency/incontinence	C M?

insignificant contribution from the cross-linking agent to overall material stiffness.

Thus, the assessment of dECM mechanical properties is important to understand and predict the cell behaviour during cell scaffold utilization. Compared to other methods, such as those that measure global scaffold mechanics (rheology and compression testing), AFM allows direct measurements of local micromechanics of scaffolds, but the results obtained depend on the tip shape (Figure 1c), as a spherical AFM tip comes to a larger contact area with the sample, than a pyramidal one and thus has lower ability to assess local differences in stiffness values [122]. In decellularized rat lung slices, Young modulus values measured with a blunted pyramidal tip were 3-fold larger than those measured with a spherical tip (Figure 1d), which could be explained with higher local strains produced by sharp tips [24]. Similar results were found at a comparison of micromechanical (measured with a spherical AFM probe with a radius of 1 μm) and nanomechanical (measured with a pyramidal AFM probe with a radius of 60 nm and) properties of decellularized aortic vessels [131]. Larger elastic moduli and wider stiffness range at the nanoscale than at the microscale level were also explained by the authors with the pyramidal probe measuring the mechanical properties of the individual components in the vascular wall rather than the global tissue properties [131].
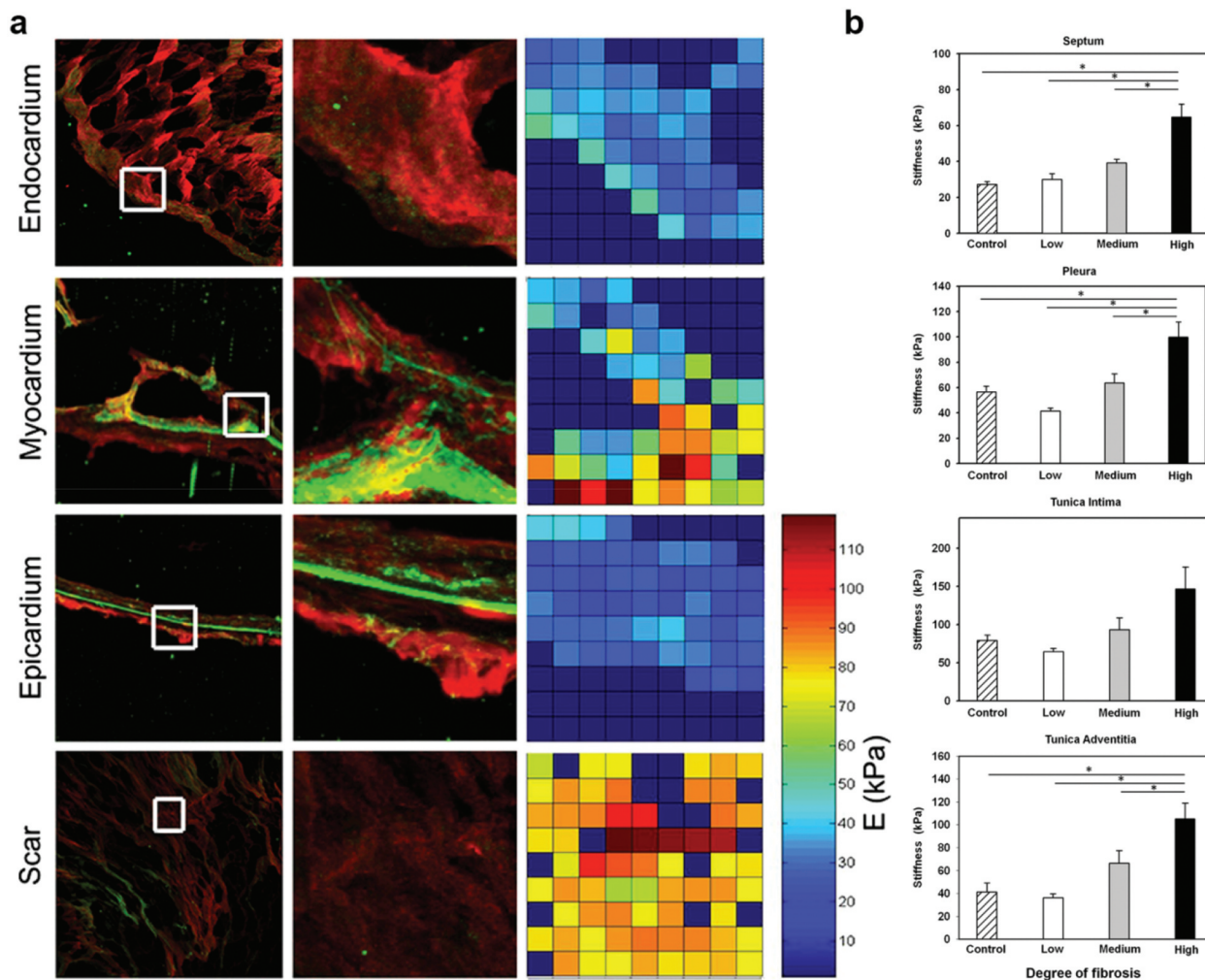
Figure 10. The stiffness in different regions of healthy and diseased heart and lung mesured by AFM. a – Fluorescence microscopy images and stiffness maps of different regions of decellularized healthy and infarcted heart. The first column demonstrates large-scale images (red – collagen I and green – elastin) with measured regions (40 μm × 40 μm) indicated by white squares. Enlarged measured regions (40 μm × 40 μm) and their stiffness maps are shown in the second and third column, respectively. (Reproduced by permission from [120], copyright [2014, Elsevier]). b – Stiffness in different locations (alveolar septa,visceralpleura,and tunicae adventitia and intima of vessels) measured by AFM in decellularized lungs of control healthy mice and mice with lung fibrosis induced by intratracheal infusion of bleomycin. The degree of fibrosis was determined as low, medium or high according to lung structural appearance (Reproduced by permission from [122], copyright [2014, Elsevier].

Local ECM stiffness sensed by cells and measured by AFM can be significantly higher than macroscale stiffness of decellularized whole tissues measured by uniaxial tensile testing. In decellularized rat lung slices, dECM was one order of magnitude stiffer at the microscale than at the macroscale, which was explained by high porosity of the lung parenchyma [24]. To study how macroscale dECM mechanics is translated into changes in microscale dECM mechanics AFM measurements were performed on decellularized rat lung slices subjected to different levels of stretch using a specially designed poly-dimethylsiloxane chip [24]. The dECM Young's modulus at the microscale increased with increasing macroscopic tissue strain, indicating that during breathing the stiffness of the alveolar cell ECM is changed in response to changes in the whole lung strain [24].

The elasticity of decellularized tissue sections can be different [29] or not significantly different [99,132] from the corresponding whole tissue sections. The variability could result from different decellularization protocols and measurement conditions, particularly whether the local or bulk tissue properties are recorded. Thus, E values of decellularized alveolar walls assessed by AFM were one order of magnitude higher than E values of whole lung tissue sections [29]. The same difference was observed in bulk mechanical properties for native and decellularized heart tissue studied by tensile tests, which was explained by absence of cells and scaffold shrinking resulting in disturbed tissue 3D structure [120]. However, the differences in local mechanical properties of native and decellularized heart tissue measured by AFM were not so large as in bulk studies [120]. According to AFM data, decellularized pancreatic tissue was slightly stiffer than the native one, but the difference was not statistically
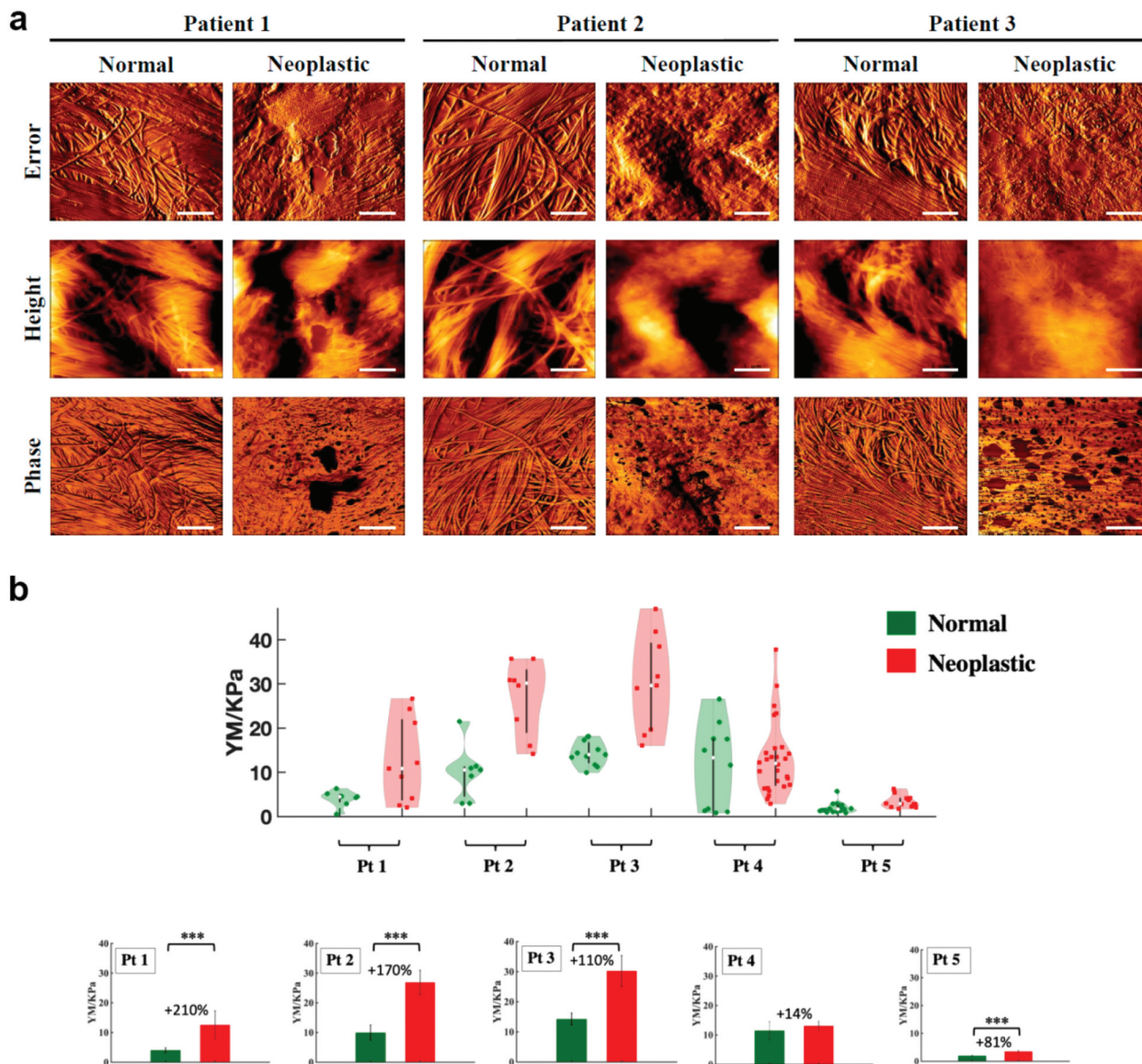
Figure 11. Morphology and mechanical properties of dECM from normal and neoplastic (peritoneal metastases of colorectal cancer) sites of the same organism. a - topography of normal and neoplastic decellularized dEcms, obtained from three different patients, visualized by AFM (phase, height, and peak force error images). Scale bar −1 μm. b - distribution of the young modulus values obtained for each patient's normal (green) and neoplastic (red) sites. Pt, patient; KPa, kilo pascal. In violin-plots, each dot represents the median young modulus value extracted from a single measurement. The bars show the mean of the median young modulus values for each patient with error bars representing effective SD of the mean. The calculated relative stiffening of the neoplastic ECM in percentages is shown. Student's t-test (**$p < 0.01$) (reproduced from [65] under the terms of the creative commons CC by license copyright [2022, Varinelli et al.]).

significant [94]. The measurement of bulk mechanical properties of decellularized arteries also showed that in comparison to native arteries, the decellularized ones were stiffer (had significantly higher tensile modulus and lower extensibility), and had decreased residual stress, which was associated with matrix structural changes [133]. In decellularized abdominal aortic vessels, the stiffnesses of the tunica media and tunica adventitia were significantly increased after decellularization, while the lumen stiffness was reduced, which was associated with ECM structure rearrangement [131].

It has been reported that cells seeded into dECM scaffolds can modify their environment [87,96]. In the AFM nanomechanical study where five types of cell scaffolds were seeded with fibroblasts and then decellularized again, it was shown that cell seeding softened the decellularized matrices (Figure 12) [87]. The seeded matrices in which the cells were grown for 14 days were less stiff than initial bare matrices, but the matrices were also softer than the bare matrices even after the cells were removed again [87]. Moreover, normal fibroblasts from healthy skin significantly softened the matrices, while diseased fibroblasts from a scar tissue and Dupuytren's fibroblasts from the palmar fascia of the same patient which also had Dupuytren's disease exerted a much smaller softening effect on the scaffold than normal fibroblasts [87].
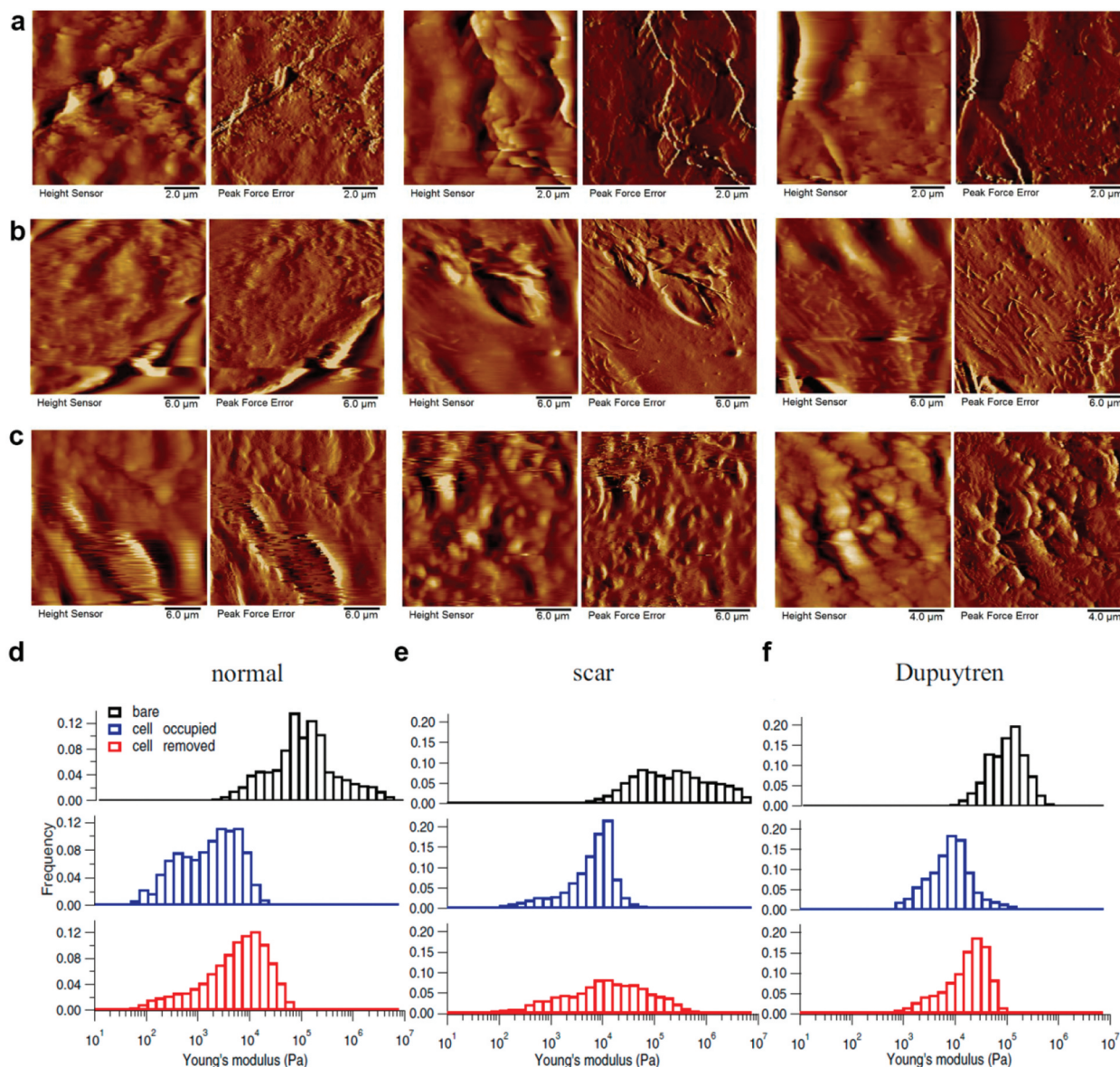
Figure 12. Changes in matrix appearance and mechanics assessed in decellularized human dermal scaffolds after seeding with normal and diseased (scar or Dupuytren's) fibroblasts of the same patient. Bare matrix (a) was seeded with primary fibroblasts isolated from normal healthy skin, from cutaneous scar tissue or from the palmar fascia affected with Dupuytren's disease (b) and then decellularized again (c). Height and PeakForce error images of bare matrices (a), matrices with normal, scar or Dupuytren's fibroblasts after two weeks of cultivation (b) and after removing the cells (c). Histograms of Young's modulus values of bare (black), cell-seeded (blue), and cell-removed matrix (red), for normal (d), scar (e) and Dupuytren's fibroblasts (f). The shifts in the histograms show the changes in matrix mechanics induced by all three fibroblast types (reproduced from [87] under a creative commons attribution 4.0 international license (http://creativecommons.org/licenses/by/4.0/) copyright [2019, Viji Babu et al.]).

The decellularization method can also potentially alter the dECM mechanical properties, as different protocols can remove various amounts of dECM essential components such as elastin [99] or glycosaminoglycan [132]. However, local matrix stiffness registered by AFM in rat lung dECM depended modestly on the decellularization procedure [119]. When local Young's modulus of the rat lung dECM at five different locations (alveolar septa, pleura, alveolar junctions, and vessels' tunica intima and tunica adventitia) obtained with four different protocols was measured using AFM, the stiffness depended much more on the site within the matrix than on the decellularization procedure [119]. However, for one location (the tunica intima), the type of the detergent (CHAPS or SDS) significantly influenced the measured Young's modulus with SDS giving almost two times higher stiffness than CHAPS [119].

Using AFM, the local micromechanics were measured in alveolar wall segments, alveolar wall junctions and pleural regions of rat lung scaffolds decellularized with sodium dodecyl sulphate [134]. The storage modulus of alveolar ECM was about 6 kPa and slightly differed between wall segments and junctions, while the stiffness of pleural regions was three times higher than that of alveolar walls. AFM studies in

decellularized pulmonary tissue of mice also confirmed that micromechanics of distinct lung anatomical compartments are different, with Young's elastic modulus (E) of stromal compartments around blood vessels (tunica intima, tunica adventitia) being 1.5–4-fold higher than that of the parenchymal compartment (i.e. alveolar septa) [28]. The inhomogeneity of dECM micromechanics of alveolar septa, pleura, and vessel's tunicae in mice lung tissue was also found by Melo et al. [122].

AFM can significantly contribute to studies of the mechanisms of cell response to ECM stimuli, as it allows separation of biochemical and mechanical cues by using bare tips or tips coated with ECM components or dECM to contact cells and measure their local mechanical response [135]. An AFM cantilever was functionalised with dECM of one of the bladder regions (submucosa, detrusor, and adventitia) cut by laser microdissection and the interactions of the AFM probes with the AY-27 rat bladder cancer cell line was studied. The differences in the adhesion of distinct dECM regions were found, corresponding to variability in composition and biophysical properties of the regions [135]. The future development of this approach could be the production of modified AFM cantilevers from patient-specific organ and tissue regions to test them against patient own cells.

9. Recent developments in dECM-based cell scaffolds

Some dECM materials are clinically approved and have been already long used for tissue restoration purposes [105,108]. Commercialized dECM products have been extensively reviewed elsewhere [3]. Here, we only briefly describe several recent studies in the field of dECM-based materials, in which AFM was involved in scaffold characterization.

The full-thickness model of human skin was obtained by bioprinting of dermis compartment with bioink made of solubilized porcine skin dECM mixed with human fibroblasts and then topped with keratinocytes as an epidermis layer [96]. The bulk mechanical properties of the model were compared to those of a skin model with dermis made of type I collagen from bovine skin. The dECM-based models had closer stiffness and viscoelasticity to excised native human skin than the collagen-based ones. However, the local organization of the fibril network revealed by AFM was different in the native skin and skin models. While in the native skin the fibrils in ECM were mostly aligned, in the skin models, the fibrils were randomly oriented (Figure 13). The stiffness and viscoelastic properties of skin models were modulated by the seeded fibroblasts, and especially keratinocytes, which synthesized human ECM proteins.

A serious problem of chondrocyte-based cartilage tissue engineering is the dedifferentiation of chondrocytes during their in vitro expansion from chondrocyte phenotypes to fibroblast phenotypes. Cell supports made of decellularized ECMs from cultured allogeneic human articular chondrocytes (AC-ECM) and bone marrow stromal cells (BM-ECM) decreased dedifferentiation and shortened the expansion time of chondrocytes in vitro as compared to chondrocytes growing on standard tissue culture polystyrene [98]. These positive effects were more prominent on dECM from allogeneic human articular chondrocytes. According to AFM analysis, the two dECM substrates differed in structure and physical properties. BM-ECM had a slightly lower Young's modulus and a rough surface with highly organized and aligned fibrils, while in AC-ECM, the fibres were not aligned and the surface was almost smooth. The BM-ECM stiffness measured by AFM appeared to be higher than that measured previously by rheometry [98]. To promote cellular migration into artificial articular cartilage implants made of porcine cartilage dECM the laser-modification technique was applied to increase the implant porosity [97].

To study in vitro the processes underlying diseases, properties of dECM hydrogels can be shifted to better correspond to those of native tissues by combining dECM with synthetic polymers. dECM derived from porcine lung was thiolated and introduced into a poly (ethylene glycol)-α-methacrylate (PEGαMA) hydrogel as a clickable dECM crosslinker to reproduce the increased stiffness of fibrotic tissues and mimic the dynamic changes in the tissue elastic moduli that occur during the disease progression [136]. Fibroblasts expressed significantly higher levels of the collagen 1a1 on the hydrogel stiff regions compared to the soft ones [136].

The bioartificial material for cartilage regeneration was obtained by growing rabbit articular chondrocytes on poly(ε-caprolactone) (PCL) electrospun fibres of different diameters (1282 ± 121 nm, 549 ± 61 nm and 285 ± 38 nm) followed by ECM decellularization [137]. The scaffold was then seeded with rabbit bone marrow-derived MSCs to study the ability of the scaffold to support stem cell adhesion, proliferation and chondrogenic differentiation. According to AFM, uncoated PCL fibres were rougher than fibres with deposited dECM. The dECM/PCL scaffolds made of 549 nm fibres were the most suited ones for MSCs chondrogenic differentiation.

dECM can be used as components to improve biocompatibility of artificial organs made of synthetic polymers; for instance, including acellularized aorta as a layer providing a collagen bed and facilitating epithelial cell growth in a PCL-based artificial trachea can help to overcome the problem of tracheal granulation after tracheostomy [138].
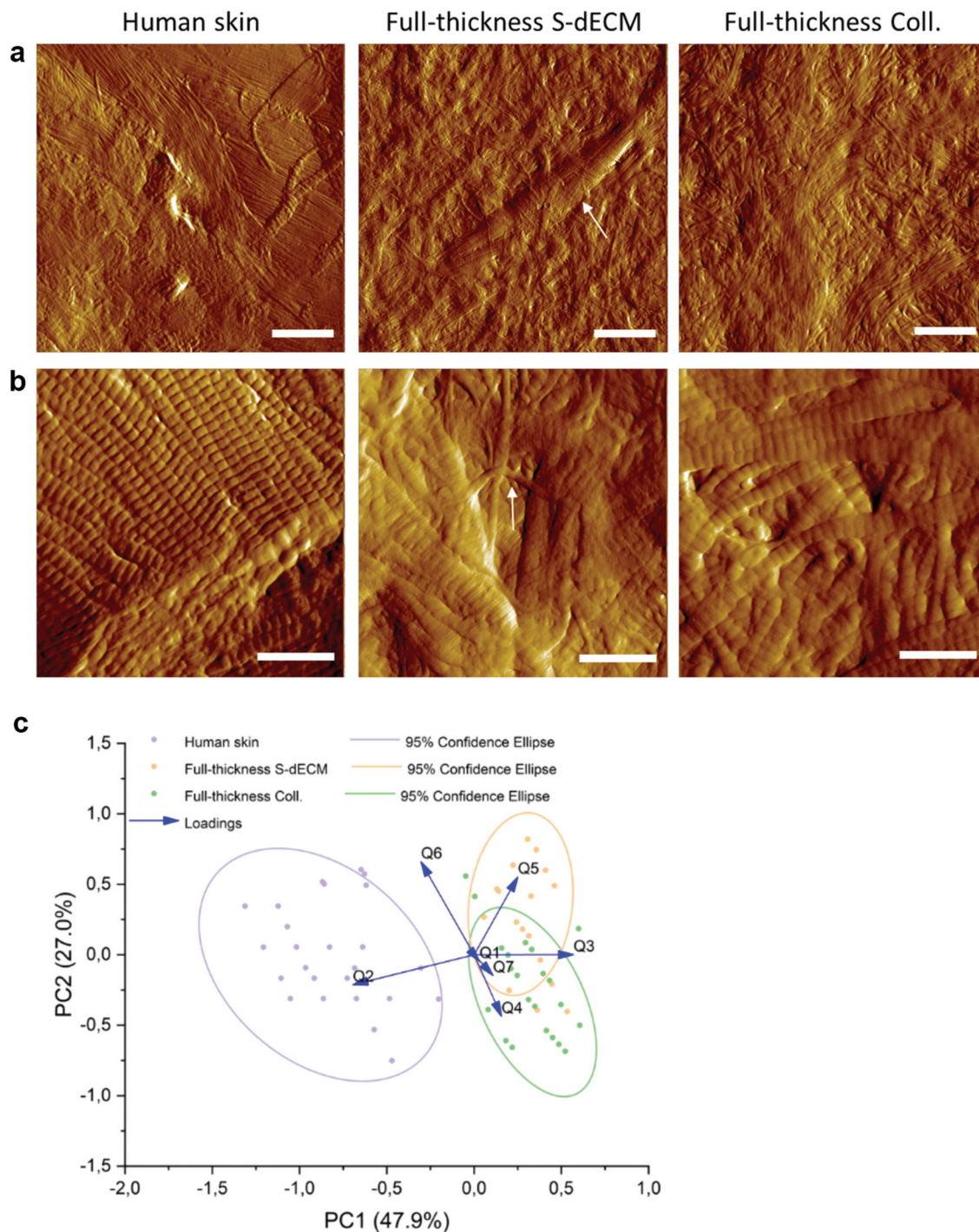
Figure 13. Organization of collagen fibrils in human and reconstructed skin models visualized by AFM. The reconstructed skin was represented by keratinocytes on top the dermis compartment made of either solubilized porcine skin dECM mixed with human fibroblasts (full-thickness S-dECM) or of type I collagen from bovine skin mixed with human fibroblasts (full-thickness coll). (a) In human skin, aligned collagen fibrils are visible, while in the two skin models fibril arrangement is disorganized. In the full-thickness S-dECM, a fiber of condensed fibrils is shown with a white arrow. Scale bar 2 μm. (b) Higher resolution AFM images (scale bar 0.5 μm) of the human and reconstructed skin, demonstrating regular periodic D-banding of collagen fibrils in all three samples. In the full-thickness S-dECM, smaller fibrils where D-banding is not discernible are shown with white arrow. (c) Principal component analysis based on AFM morphological scores demonstrates that human skin morphology differs from those of the two models, and the skin models also differ from one another (reproduced by permission from [96], copyright [2022, Elsevier]).

The field of dECM-based materials for tissue engineering is growing. Decellularization of various tissues and organs including liver [139], bone and cartilage [49] pancreas [94], skeletal muscle [140], kidney [141], bladder muscle, heart valve, and limb [94] has already been performed. However, the search for safer decellularization techniques that allow better preservation of ECM structure, mechanics and thus functionality is continuing. As AFM technique supplies unique data on dECM nanostructure and mechanics, thorough characterization of dECM properties with AFM can help to

reveal structure–function relationships in health and disease.

10. Conclusion

Acellular tissues, organs and cell cultures have been exploited as ready-to-use cell scaffolds, which reproduce a large part of structural, mechanical and chemical traits of the native ECM. However, some ECM components are lost or damaged during decellularization, thus necessitating further improvement of decellularization procedures in a tissue-specific manner. AFM can observe geometrical and mechanical characteristics of obtained dECM scaffolds both at the level of individual ECM components (such as collagen fibres and proteoglycan molecules) and at the level of supramolecular assemblies, depending on the instrument operation parameters. We expect that application of AFM for characterizing dECM-based materials will grow in the future due to the high instrument versatility. A wide range of information can be obtained by a properly designed AFM analysis including the choice of cantilever tip size and shape, cantilever modification with specific substances (including ECM components and whole dECM) and raw data treatment methods. Therefore, in addition to simply assessing the ECM preservation after decellularization, AFM can contribute to studies of structure–function relationship between the physical properties of cell microenvironment and their influence on the cell behavior under healthy and diseased conditions.

Disclosure statement

No potential conflict of interest was reported by the author(s).

Funding

Notes on contributors

Svetlana Batasheva studied biochemistry at the Kazan State University, Russian Federation, from which she graduated in 2003. She obtained her PhD degree in 2006 from Kazan Institute of Biochemistry and Biophysics of the Russian Academy of Sciences. In 2016 she joined the research group of Prof. Rawil Fakhrullin as a senior research scientist. Her current research interests include obtaining functional composites

based on nanoparticles and biopolymers, and nanotoxicology.

Svetlana Kotova obtained her MSc degree in Chemistry (1994) from the Moscow State University, Department of Chemistry, Russian Federation. In 2004, she was awarded a Doctorate Degree in Solid State Chemistry from the L. Y. Karpov Research Institute of Physical Chemistry, Moscow, Russian Federation. She is currently appointed as a Leading Researcher at the Sechenov University, Russian Federation. Her current research interests include: 1) biological and biomedical applications of atomic force microscopy; 2) physical chemistry and mechanics of thermoresponsive polymer materials; 3) mechanical properties of scaffold materials for tissue engineering; 4) physicochemical and rheological properties of thermoresponsive gels.

Anastasia Frolova obtained her MSc degree in Chemical Technology (2018) from the Russian Technological University, Institute of Fine Chemical Technology, Moscow, Russian Federation. She is currently appointed as a Head of the Laboratory of Correlation Microscopy at the Sechenov University, Russian Federation. Her current research interests include: 1) surface structure features of materials using correlation microscopy; 2) biological and biomedical applications of atomic force and scanning electron microscopy; 3) phase and mechanical behaviour of thermoresponsive polymer materials; 4) biomechanical properties of scaffold materials for tissue engineering.

Rawil Fakhrullin received his MSc (2003) and PhD (2006) degrees in biochemistry from Kazan State University. Currently, he is a principal investigator at the Institute of fundamental biology and medicine, Kazan Federal University (Republic of Tatarstan, Russian Federation), and professor at the Sechenov University and Tomsk State University. His research interests are focused on nanoclay-based materials for biomedical applications; environmental pollution and remediation; and advanced microscopy techniques for bioanalytical application and colloid chemistry. He is a Fellow of the Royal Society of Chemistry since 2017.

ORCID

Svetlana Batasheva http://orcid.org/0000-0002-9510-3832
Svetlana Kotova http://orcid.org/0000-0001-7011-4503
Anastasia Frolova http://orcid.org/0000-0003-1073-2611
Rawil Fakhrullin http://orcid.org/0000-0003-2015-7649

References

[1] Tonti OR, Larson H, Lipp SN, et al. Tissue-specific parameters for the design of ecm-mimetic

biomaterials. Acta Biomater. 2021;132:83–102. doi: 10.1016/j.actbio.2021.04.017

[2] Unal AZ, West JL. Synthetic ECM: bioactive synthetic hydrogels for 3D tissue engineering. Bioconjug Chem. 2020;31(10):2253–2271. doi: 10.1021/acs.bioconjchem.0c00270

[3] Liao J, Xu B, Zhang R, et al. Applications of decellularized materials in tissue engineering: advantages, drawbacks and current improvements, and future perspectives. J Mater Chem B. 2020;8(44):10023–10049. doi: 10.1039/D0TB01534B

[4] Neishabouri A, Soltani Khaboushan A, Daghigh F, et al. Decellularization in tissue engineering and regenerative medicine: evaluation, modification, and application methods. Front Bioeng Biotechnol. 2022;10:805299. doi: 10.3389/fbioe.2022.805299

[5] Yip LX, Wang J, Xue Y, et al. Cell-derived nanomaterials for biomedical applications. Sci Technol Adv Mater. 2024;25(1):2315013. doi: 10.1080/14686996.2024.2315013

[6] Ariga K, Fakhrullin R. Materials nanoarchitectonics from atom to living cell: a method for everything. Bull Chem Soc Jpn. 2022;95(5):774–795. doi: 10.1246/bcsj.20220071

[7] Yang B, Wei K, Loebel C, et al. Enhanced mechanosensing of cells in synthetic 3D matrix with controlled biophysical dynamics. Nat Commun. 2021;12(1):3514. doi: 10.1038/s41467-021-23120-0

[8] Matsusaki M, Kadowaki K, Nakahara Y, et al. Fabrication of cellular multilayers with nanometer-sized extracellular matrix films. Angew Chem Int Ed Engl. 2007;46(25):4689–4692. doi: 10.1002/anie.200701089

[9] Lou J, Stowers R, Nam S, et al. Stress relaxing hyaluronic acid-collagen hydrogels promote cell spreading, fiber remodeling, and focal adhesion formation in 3D cell culture. Biomaterials. 2018;154:213–222. doi: 10.1016/j.biomaterials.2017.11.004

[10] Hwang JH, Han U, Yang M, et al. Artificial cellular nano-environment composed of collagen-based nanofilm promotes osteogenic differentiation of mesenchymal stem cells. Acta Biomater. 2019;86:247–256. doi: 10.1016/j.actbio.2018.12.044

[11] Zeng J, Matsusaki M. Layer-by-layer assembly of nanofilms to control cell functions. Polym Chem. 2019;10(23):2960–2974. doi: 10.1039/C9PY00305C

[12] Jia X, Chen J, Lv W, et al. Engineering dynamic and interactive biomaterials using material nanoarchitectonics for modulation of cellular behaviors. Cell Rep Phys Sci. 2023;4(2):101251. doi: 10.1016/j.xcrp.2023.101251

[13] Graham HK, Hodson NW, Hoyland JA, et al. Tissue section AFM: In situ ultrastructural imaging of native biomolecules. Matrix Biol. 2010;29(4):254–260. doi: 10.1016/j.matbio.2010.01.008

[14] Tello M, Spenlé C, Hemmerlé J, et al. Generating and characterizing the mechanical properties of cell-derived matrices using atomic force microscopy. Methods. 2016;94:85–100. doi: 10.1016/j.ymeth.2015.09.012

[15] Liu J, Song Q, Yin W, et al. Bioactive scaffolds for tissue engineering: a review of decellularized extracellular matrix applications and innovations. Exploration. 2024:20230078.

[16] Golebiowska AA, Intravaia JT, Sathe VM, et al. Decellularized extracellular matrix biomaterials for regenerative therapies: advances, challenges and clinical prospects. Bioact Mater. 2024;32:98–123. doi: 10.1016/j.bioactmat.2023.09.017

[17] Jorba I, Uriarte JJ, Campillo N, et al. Probing micromechanical properties of the extracellular matrix of soft tissues by atomic force microscopy. J Cell Physiol. 2017;232(1):19–26. doi: 10.1002/jcp.25420

[18] Ushiki T, Hoshi O. Atomic force microscopy for imaging human metaphase chromosomes. Chromosome Res. 2008;16(3):383–396. doi: 10.1007/s10577-008-1241-7

[19] Perrino AP, Miyagi A, Scheuring S. Single molecule kinetics of bacteriorhodopsin by HS-AFM. Nat Commun. 2021;12(1):7225. doi: 10.1038/s41467-021-27580-2

[20] Witz G, Stasiak A. DNA supercoiling and its role in DNA decatenation and unknotting. Nucleic Acids Res. 2010;38(7):2119–2133. doi: 10.1093/nar/gkp1161

[21] Frolova A, Aksenova N, Novikov I, et al. A collagen basketweave from the giant squid mantle as a robust scaffold for tissue engineering. Mar Drugs. 2021;19(12):679. doi: 10.3390/md19120679

[22] Kilpatrick JI, Revenko I, Rodriguez BJ. Nanomechanics of cells and biomaterials studied by atomic force microscopy. Adv Healthc Mater. 2015;4(16):2456–2474. doi: 10.1002/adhm.201500229

[23] Gavara N. A beginner's guide to atomic force microscopy probing for cell mechanics. Microsc Res Tech. 2017;80(1):75–84. doi: 10.1002/jemt.22776

[24] Jorba I, Beltrán G, Falcones B, et al. Nonlinear elasticity of the lung extracellular microenvironment is regulated by macroscale tissue strain. Acta Biomater. 2019;92:265–276. doi: 10.1016/j.actbio.2019.05.023

[25] Moeendarbary E, Harris AR. Cell mechanics: principles, practices, and prospects. WIREs Syst Biol Med. 2014;6(5):371–388. doi: 10.1002/wsbm.1275

[26] Efremov YM, Bagrov DV, Dubrovin EV, et al. Atomic force microscopy of animal cells: advances and prospects. Biophysics. 2011;56(2):257–267. doi: 10.1134/S0006350911020096

[27] Efremov YM, Bakhchieva NA, Shavkuta BS, et al. Mechanical properties of anterior lens capsule assessed with AFM and nanoindenter in relation to human aging, pseudoexfoliation syndrome, and trypan blue staining. J Mech Behav Biomed Mater. 2020;112:104081. doi: 10.1016/j.jmbbm.2020.104081

[28] Alcaraz J, Otero J, Jorba I, et al. Bidirectional mechanobiology between cells and their local extracellular matrix probed by atomic force microscopy. Semin Cell Dev Biol. 2018;73:71–81. doi: 10.1016/j.semcdb.2017.07.020

[29] Giménez A, Uriarte JJ, Vieyra J, et al. Elastic properties of hydrogels and decellularized tissue sections used in mechanobiology studies probed by atomic force microscopy. Microsc Res Tech. 2017;80(1):85–96. doi: 10.1002/jemt.22740

[30] Acerbi I, Luque T, Giménez A, et al. Integrin-specific mechanoresponses to compression and extension probed by cylindrical flat-ended AFM tips in lung cells. PloS One. 2013;7(2). doi: 10.1371/journal.pone.0032261

[31] Kotova SL, Timashev PS, Guller AE, et al. Collagen hierarchical structure deterioration in the skin of patients with pelvic organ prolapse tracked by atomic force microscopy. Microsc Microanal. 2015;21(2):324–333. doi: 10.1017/S1431927615000148

[32] Gubar'kova EV, Kirillin MY, Dudenkova VV, et al. Quantitative evaluation of atherosclerotic plaques

using cross-polarization optical coherence tomography, nonlinear, and atomic force microscopy. J Biomed Opt. 2016;21(12):126010. doi: 10.1117/1. JBO.21.12.126010

[33] Ţălu Ş, Stach S, Sueiras V, et al. Fractal analysis of AFM images of the surface of Bowman's membrane of the human cornea. Ann Biomed Eng. 2015;43 (4):906–916. doi: 10.1007/s10439-014-1140-3

[34] Timashev PS, Kotova SL, Belkova GV, et al. Atomic force microscopy study of atherosclerosis progression in arterial walls. Microsc Microanal. 2016;22 (2):311–325. doi: 10.1017/S1431927616000039

[35] Kiseleva EB, Gubarkova EV, Dudenkova VV, et al. Complementary study of collagen state in bladder diseases using cross-polarization optical coherence tomography, nonlinear and atomic force microscopy. Sovrem Tehnol Med. 2017;9(1):7–20. doi: 10.17691/stm2017.9.1.01

[36] Kotova SL, Timashev PS, Belkova GV, et al. Early effects of ionizing radiation on the collagen hierarchical structure of bladder and rectum visualized by atomic force microscopy. Microsc Microanal. 2018;24(1):38–48. doi: 10.1017/S1431927618000065

[37] Timashev PS, Koroleva AV, Konovalov NA, et al. Atomic force microscopy of tissue sections is a useful complementary tool in biomedical morphological studies. Sovremennye tehnologii v Med. 2018;10(1):70–80. doi: 10.17691/stm2018.10.1.09

[38] Kargin NI, Gusev AS, Ryndya SM, et al. Visualization of supersmooth surfaces texture by the method of flicker-noise spectroscopy. Sci Visual. 2017;9 (3):28–41. Available from: https://sv-journal.org/ 2017-3/03.php?lang=en

[39] Timashev SF. Flicker noise spectroscopy and its application: information hidden in chaotic signals (review). Russ J Electrochem. 2006;42(5):424–466. doi: 10.1134/S102319350605003X

[40] Mirsaidov U, Timashev SF, Polyakov Y, et al. Analytical method for parameterizing the random profile components of nanosurfaces imaged by atomic force microscopy. Analyst. 2011;136 (3):570–576. doi: 10.1039/C0AN00498G

[41] Telesca L, Lapenna V, Timashev S, et al. Flicker-noise spectroscopy: a new approach to investigate the time dynamics of geoelectrical signals measured in seismic areas. Phys Chem Earth. 2004;29(4–9):389–395. doi: 10.1016/j.pce.2003.09.017

[42] Abdullaev NT, Dyshin OA, Gasankulieva MM. Flicker noise spectroscopy of electrocardiographic signals. Biomed Eng. 2016;49(5):268–273. doi: 10. 1007/s10527-016-9546-x

[43] Broniec A. Analysis of EEG signal by flicker-noise spectroscopy: identification of right-/left-hand movement imagination. Med Biol Eng Comput. 2016;54 (12):1935–1947. doi: 10.1007/s11517-016-1491-z

[44] Demin S, Panischev O, Yunusov V, et al. The use of flicker-noise spectroscopy in the diagnosis of photosensitive epilepsy based on the analysis of human magnetoencephalograms. In: Proceedings of the VI International Conference on Information Technology and Nanotechnology (ITNT-2020); 2020 May 26–29; Samara, Russia. Vol. 2020. p. 1–4. 10 .1109/ ITNT49337.2020.9253221.

[45] Drabik D, Przybyło M, Chodaczek G, et al. The modified fluorescence based vesicle fluctuation spectroscopy technique for determination of lipid bilayer bending properties. Biochim Biophys Acta.

2016;1858(2):244–252. doi: 10.1016/j.bbamem.2015. 11.020

[46] Doskocz J, Drabik D, Chodaczek G, et al. Statistical analysis of bending rigidity coefficient determined using fluorescence-based flicker-noise spectroscopy. J Membr Biol. 2018;251(4):601–608. doi: 10.1007/ s00232-018-0037-8

[47] Wang H, Zhang H, Tamura R, et al. Mapping stress inside living cells by atomic force microscopy in response to environmental stimuli. Sci Technol Adv Mater. 2023;24(1):2265434. doi: 10.1080/14686996. 2023.2265434

[48] Yao Q, Zheng YW, Lan QH, et al. Recent development and biomedical applications of decellularized extracellular matrix biomaterials. Mater Sci Eng C. 2019;104:109942. doi: 10.1016/j.msec.2019.109942

[49] Kim YS, Majid M, Melchiorri AJ, et al. Applications of decellularized extracellular matrix in bone and cartilage tissue engineering. Bioeng Transl Med. 2019;4(1):83–95. doi: 10.1002/btm2.10110

[50] Yusen RD, Shearon TH, Qian Y, et al. Lung transplantation in the United States, 1999–2008. Am J Transplant. 2010;10(4):1047–1068. doi: 10.1111/j. 1600-6143.2010.03055.x

[51] McInnes AD, Moser MA, Chen X. Preparation and use of decellularized extracellular matrix for tissue engineering. J Funct Biomater. 2022;13(4):240. doi: 10.3390/jfb13040240

[52] Shakouri-Motlagh A, O'Connor AJ, Brennecke SP, et al. Native and solubilized decellularized extracellular matrix: a critical assessment of their potential for improving the expansion of mesenchymal stem cells. Acta Biomater. 2017;55:1–12. doi: 10.1016/j.actbio. 2017.04.014

[53] Hoshiba T. Cultured cell-derived decellularized matrices: a review towards the next decade. J Mater Chem B. 2017;5(23):4322–4331. doi: 10.1039/ C7TB00074J

[54] Hussein KH, Park KM, Yu L, et al. Vascular reconstruction: a major challenge in developing a functional whole solid organ graft from decellularized organs. Acta Biomater. 2020;103:68–80. doi: 10. 1016/j.actbio.2019.12.029

[55] Abaci A, Guvendiren M. Designing decellularized extracellular matrix-based bioinks for 3D bioprinting. Adv Healthc Mater. 2020;9(24):2000734. doi: 10. 1002/adhm.202000734

[56] Kim BS, Das S, Jang J, et al. Decellularized extracellular matrix-based bioinks for engineering tissue-and organ-specific microenvironments. Chem Rev. 2020;120(19):10608–10661. doi: 10.1021/acs.chem rev.9b00808

[57] Saldin LT, Cramer MC, Velankar SS, et al. Extracellular matrix hydrogels from decellularized tissues: Structure and function. Acta Biomater. 2017;49:1–15. doi: 10.1016/j.actbio.2016.11.068

[58] Ibsirlioglu T, Elçin AE, Elçin YM. Decellularized biological scaffold and stem cells from autologous human adipose tissue for cartilage tissue engineering. Methods. 2020;171:97–107. doi: 10. 1016/j.ymeth.2019.04.020

[59] Anasiz Y, Ozgul RK, Uckan-Cetinkaya D. A new chapter for mesenchymal stem cells: decellularized extracellular matrices. STEM Cell Rev Rep. 2017;13 (5):587–597. doi: 10.1007/s12015-017-9757-x

[60] Yang MC, O'Connor AJ, Kalionis B, et al. Improvement of mesenchymal stromal cell

proliferation and differentiation via decellularized extracellular matrix on substrates with a range of surface chemistries. Front Med Technol. 2022;4:834123. doi: 10.3389/fmedt.2022.834123

[61] Pernodet N, Rafailovich M, Sokolov J, et al. Fibronectin fibrillogenesis on sulfonated polystyrene surfaces. J Biomed Mater Res. 2003;64A(4):684–692. doi: 10.1002/jbm.a.10394

[62] Soucy PA, Werbin J, Heinz W, et al. Microelastic properties of lung cell-derived extracellular matrix. Acta Biomater. 2011;7(1):96–105. doi: 10.1016/j.actbio.2010.07.021

[63] Bourgine PE, Gaudiello E, Pippenger B, et al. Engineered extracellular matrices as biomaterials of tunable composition and function. Adv Funct Mater. 2017;27(7):1605486. doi: 10.1002/adfm.201605486

[64] Sani M, Hosseinie R, Latifi M, et al. Engineered artificial articular cartilage made of decellularized extracellular matrix by mechanical and IGF-1 stimulation. Biomater Adv. 2022;139:213019. doi: 10.1016/j.bioadv.2022.213019

[65] Varinelli L, Guaglio M, Brich S, et al. Decellularized extracellular matrix as scaffold for cancer organoid cultures of colorectal peritoneal metastases. J Mol Cell Biol. 2022;14(11):mjac064. doi: 10.1093/jmcb/mjac064

[66] Quansah E, Shaik TA, Çevik E, et al. Investigating biochemical and structural changes of glycated collagen using multimodal multiphoton imaging, Raman spectroscopy, and atomic force microscopy. Anal Bioanal Chem. 2023;415(25):6257–6267. doi: 10.1007/s00216-023-04902-5

[67] Willemse J, van Tienderen G, van Hengel E, et al. Hydrogels derived from decellularized liver tissue support the growth and differentiation of cholangiocyte organoids. Biomaterials. 2022;284:121473. doi: 10.1016/j.biomaterials.2022.121473

[68] Kim S, Min S, Choi YS, et al. Tissue extracellular matrix hydrogels as alternatives to matrigel for culturing gastrointestinal organoids. Nat Commun. 2022;13(1):1–21. doi: 10.1038/s41467-022-29279-4

[69] van Tienderen GS, Conboy J, Muntz I, et al. Tumor decellularization reveals proteomic and mechanical characteristics of the extracellular matrix of primary liver cancer. Biomater Adv. 2023;146:213289. doi: 10.1016/j.bioadv.2023.213289

[70] Booth AJ, Hadley R, Cornett AM, et al. Acellular normal and fibrotic human lung matrices as a culture system for in vitro investigation. Amer J Respir Crit Care Med. 2012;186(9):866–876. doi: 10.1164/rccm.201204-0754OC

[71] Birk DE, Bruckner P. Collagen suprastructures. Top Curr Chem. 2005;247:185–205.

[72] Abraham LC, Zuena E, Perez-Ramirez B, et al. Guide to collagen characterization for biomaterial studies. J Biomed Mater Res. 2008;87B(1):264–285. doi: 10.1002/jbm.b.31078

[73] Cauble MA, Mancini NS, Kalinowski J, et al. Atomic force microscopy imaging for nanoscale and microscale assessments of extracellular matrix in intervertebral disc and degeneration. JOR Spine. 2020;3(3):e1125. doi: 10.1002/jsp2.1125

[74] Ng L, Grodzinsky AJ, Patwari P, et al. Individual cartilage aggrecan macromolecules and their constituent glycosaminoglycans visualized via atomic force microscopy. J Struct Biol. 2003;143(3):242–257. doi: 10.1016/j.jsb.2003.08.006

[75] Asgari M, Latifi N, Giovanniello F, et al. Revealing layer-specific ultrastructure and nanomechanics of fibrillar collagen in human aorta via atomic force microscopy testing: implications on tissue mechanics at macroscopic scale. Adv NanoBiomed Res. 2022;2(5):2100159. doi: 10.1002/anbr.202100159

[76] Moo EK, Ebrahimi M, Sibole SC, et al. The intrinsic quality of proteoglycans, but not collagen fibres, degrades in osteoarthritic cartilage. Acta Biomater. 2022;153:178–189. doi: 10.1016/j.actbio.2022.09.002

[77] Wagenseil JE, Mecham RP. New insights into elastic fiber assembly. Birth Defects Res C Embryo Today. 2007;81(4):229–240. doi: 10.1002/bdrc.20111

[78] Khan SA, Mason RW, Kobayashi H, et al. Advances in glycosaminoglycan detection. Mol Genet Metab. 2020;130(2):101–109. doi: 10.1016/j.ymgme.2020.03.004

[79] Soares da Costa D, Reis RL, Pashkuleva I. Sulfation of glycosaminoglycans and its implications in human health and disorders. Annu Rev Biomed Eng. 2017;19(1):1–26. doi: 10.1146/annurev-bioeng-071516-044610

[80] Seog J, Dean D, Plaas AHK, et al. Direct measurement of glycosaminoglycan intermolecular interactions via high-resolution force spectroscopy. Macromolecules. 2002;35(14):5601–5615. doi: 10.1021/ma0121621

[81] Uhl FE, Zhang F, Pouliot RA, et al. Functional role of glycosaminoglycans in decellularized lung extracellular matrix. Acta Biomater. 2020;102:231–246. doi: 10.1016/j.actbio.2019.11.029

[82] Subburaman K, Pernodet N, Kwak SY, et al. Templated biomineralization on self-assembled protein fibers. Proc Natl Acad Sci USA. 2006;103(40):14672–14677. doi: 10.1073/pnas.0602952103

[83] Sambani K, Kontomaris SV, Yova D. Atomic force microscopy imaging of elastin nanofibers self-assembly. Materials. 2023;16(12):4313. doi: 10.3390/ma16124313

[84] Raspanti M, Congiu T, Alessandrini A, et al. Different patterns of collagen-proteoglycan interaction: a scanning electron microscopy and atomic force microscopy study. Eur J Histochem. 2000;44(4):335–344.

[85] Schoenenberger MS, Halfter W, Ferrand A, et al. The biophysical and compositional properties of human basement membranes. FEBS J. 2024;291(3):477–488. doi: 10.1111/febs.17007

[86] Liguori GR, Liguori TTA, de Moraes SR, et al. Molecular and biomechanical clues from cardiac tissue decellularized extracellular matrix drive stromal cell plasticity. Front Bioeng Biotechnol. 2020;8:520. doi: 10.3389/fbioe.2020.00520

[87] Viji Babu PK, Rianna C, Mirastschijski U, et al. Nanomechanical mapping of interdependent cell and ECM mechanics by AFM force spectroscopy. Sci Rep. 2019;9(1):12317. doi: 10.1038/s41598-019-48566-7

[88] Wen CY, Wu CB, Tang B, et al. Collagen fibril stiffening in osteoarthritic cartilage of human beings revealed by atomic force microscopy. Osteoarthritis Cartilage. 2012;20(8):916–922. doi: 10.1016/j.joca.2012.04.018

[89] Jones B, Tonniges JR, Debski A, et al. Collagen fibril abnormalities in human and mice abdominal aortic aneurysm. Acta Biomater. 2020;110:129–140. doi: 10.1016/j.actbio.2020.04.022

[90] Berquand A, Wahart A, Henry A, et al. Revealing the elasticity of an individual aortic fiber during ageing at

nanoscale by in situ atomic force microscopy. Nanoscale. 2021;13(2):1124–1133. doi: 10.1039/D0NR06753A

[91] Zambon JP, Atala A, Yoo JJ. Methods to generate tissue-derived constructs for regenerative medicine applications. Methods. 2020;171:3–10. doi: 10.1016/j.ymeth.2019.09.016

[92] Yang J, Dang H, Xu Y. Recent advancement of decellularization extracellular matrix for tissue engineering and biomedical application. Artif Organs. 2022;46(4):549–567. doi: 10.1111/aor.14126

[93] Cartmell JS, Dunn MG. Effect of chemical treatments on tendon cellularity and mechanical properties. J Biomed Mater Res. 2000;49(1):134–140. doi: 10.1002/(SICI)1097-4636(200001)49:1<134::AID-JBM17>3.0.CO;2-D

[94] Singh G, Senapati S, Satpathi S, et al. Establishment of decellularized extracellular matrix scaffold derived from caprine pancreas as a novel alternative template over porcine pancreatic scaffold for prospective biomedical application. FASEB J. 2022;36(10):e22574. doi: 10.1096/fj.202200807R

[95] Łabuś W, Glik J, Klama-Baryła A, et al. Atomic force microscopy in the production of a biovital skin graft based on human acellular dermal matrix produced in-house and in vitro cultured human fibroblasts. J Biomed Mater Res B Appl Biomater. 2018;106(2):726–733. doi: 10.1002/jbm.b.33883

[96] Girardeau-Hubert S, Lynch B, Zuttion F, et al. Impact of microstructure on cell behavior and tissue mechanics in collagen and dermal decellularized extra-cellular matrices. Acta Biomater. 2022;143:100–114. doi: 10.1016/j.actbio.2022.02.035

[97] Li Y, Xu Y, Liu Y, et al. Decellularized cartilage matrix scaffolds with laser-machined micropores for cartilage regeneration and articular cartilage repair. Mater Sci Eng C Mater Biol Appl. 2019;105:110139. doi: 10.1016/j.msec.2019.110139

[98] Mao Y, Block T, Singh-Varma A, et al. Extracellular matrix derived from chondrocytes promotes rapid expansion of human primary chondrocytes in vitro with reduced dedifferentiation. Acta Biomater. 2019;85:75–83. doi: 10.1016/j.actbio.2018.12.006

[99] Narciso M, Ulldemolins A, Júnior C, et al. Novel decellularization method for tissue slices. Front Bioeng Biotechnol. 2022;10:832178. doi: 10.3389/fbioe.2022.832178

[100] Rao Pattabhi S, Martinez JS, Keller TC. 3rd. Decellularized ECM effects on human mesenchymal stem cell stemness and differentiation. Differentiation. 2014;88(4–5):131–143. doi: 10.1016/j.diff.2014.12.005

[101] Novoseletskaya E, Grigorieva O, Nimiritsky P, et al. Mesenchymal stromal cell-produced components of extracellular matrix potentiate multipotent stem cell response to differentiation stimuli. Front Cell Dev Biol. 2020;8:555378. doi: 10.3389/fcell.2020.555378

[102] Song YH, Maynes MA, Hlavac N, et al. Development of novel apoptosis-assisted lung tissue decellularization methods. Biomater Sci. 2021;9(9):3485–3498. doi: 10.1039/D1BM00032B

[103] Kasravi M, Ahmadi A, Babajani A, et al. Immunogenicity of decellularized extracellular matrix scaffolds: a bottleneck in tissue engineering and regenerative medicine. Biomater Res. 2023;27(1):10. doi: 10.1186/s40824-023-00348-z

[104] Gilbert TW, Freund JM, Badylak SF. Quantification of DNA in biologic scaffold materials. J Surg Res. 2009;152(1):135–139. doi: 10.1016/j.jss.2008.02.013

[105] Aamodt JM, Grainger DW. Extracellular matrix-based biomaterial scaffolds and the host response. Biomaterials. 2016;86:68–82. doi: 10.1016/j.biomaterials.2016.02.003

[106] Zhang X, Chen X, Hong H, et al. Decellularized extracellular matrix scaffolds: recent trends and emerging strategies in tissue engineering. Bioact Mater. 2022;10:15–31. doi: 10.1016/j.bioactmat.2021.09.014

[107] Arzi B, DuRaine GD, Lee CA, et al. Cartilage immunoprivilege depends on donor source and lesion location. Acta Biomater. 2015;23:72–81. doi: 10.1016/j.actbio.2015.05.025

[108] Kawecki M, Łabuś W, Klama-Baryla A, et al. A review of decellurization methods caused by an urgent need for quality control of cell-free extracellular matrix'scaffolds and their role in regenerative medicine. J Biomed Mater Res Part B Appl Biomater. 2018;106(2):909–923. doi: 10.1002/jbm.b.33865

[109] Rowland CR, Colucci LA, Guilak F. Fabrication of anatomically-shaped cartilage constructs using decellularized cartilage-derived matrix scaffolds. Biomaterials. 2016;91:57–72. doi: 10.1016/j.biomaterials.2016.03.012

[110] Ye X, Wang H, Gong W, et al. Impact of decellularization on porcine myocardium as scaffold for tissue engineered heart tissue. J Mater Sci Mater Med. 2016;27(4):70. doi: 10.1007/s10856-016-5683-8

[111] Lo CM, Wang HB, Dembo M, et al. Cell movement is guided by the rigidity of the substrate. Biophys J. 2000;79(1):144–152. doi: 10.1016/S0006-3495(00)76279-5

[112] Discher DE, Janmey P, Wang YL. Tissue cells feel and respond to the stiffness of their substrate. Science. 2005;310(5751):1139–1143. doi: 10.1126/science.1116995

[113] Yeung T, Georges PC, Flanagan LA, et al. Effects of substrate stiffness on cell morphology, cytoskeletal structure, and adhesion. Cell Motil Cytoskeleton. 2005;60(1):24–34. doi: 10.1002/cm.20041

[114] Paszek MJ, Zahir N, Johnson KR, et al. Tensional homeostasis and the malignant phenotype. Cancer Cell. 2005;8(3):241–254. doi: 10.1016/j.ccr.2005.08.010

[115] Ingber D. Mechanobiology and diseases of mechanotransduction. Ann Med. 2003;35(8):564–577. doi: 10.1080/07853890310016333

[116] Engler AJ, Carag-Krieger C, Johnson CP, et al. Embryonic cardiomyocytes beat best on a matrix with heart-like elasticity: scar-like rigidity inhibits beating. J Cell Sci. 2008;121(22):3794–3802. doi: 10.1242/jcs.029678

[117] Yi B, Xu Q, Liu W. An overview of substrate stiffness guided cellular response and its applications in tissue regeneration. Bioact Mater. 2022;15:82–102. doi: 10.1016/j.bioactmat.2021.12.005

[118] Engler AJ, Sen S, Sweeney HL, et al. Matrix elasticity directs stem cell lineage specification. Cell. 2006;126(4):677–689. doi: 10.1016/j.cell.2006.06.044

[119] Melo E, Garreta E, Luque T, et al. Effects of the decellularization method on the local stiffness of acellular lungs. Tissue Eng Part C Methods. 2014;20(5):412–422. doi: 10.1089/ten.tec.2013.0325

[120] Andreu I, Luque T, Sancho A, et al. Heterogeneous micromechanical properties of the extracellular matrix in healthy and infarcted hearts. Acta

Biomater. 2014;10(7):3235–3242. doi: 10.1016/j.act bio.2014.03.034

[121] Holuigue H, Lorenc E, Chighizola M, et al. Force sensing on cells and tissues by atomic force microscopy. Sensors. 2022;22(6):2197. doi: 10.3390/s22062197

[122] Melo E, Cárdenes N, Garreta E, et al. Inhomogeneity of local stiffness in the extracellular matrix scaffold of fibrotic mouse lungs. J Mech Behav Biomed Mater. 2014;37:186–195. doi: 10.1016/j.jmbbm.2014.05.019

[123] Marques-Magalhães Â, Cruz T, Costa ÂM, et al. Decellularized colorectal cancer matrices as bioactive scaffolds for studying tumor-stroma interactions. Cancers (Basel). 2022;14(2):359. doi: 10.3390/cancers14020359

[124] Fernandez-Sanchez ME, Barbier S, Whitehead J, et al. Mechanical induction of the tumorigenic β-catenin pathway by tumour growth pressure. Nature. 2015;523(7558):92–95. doi: 10.1038/nature14329

[125] Bauer J, Emon MAB, Staudacher JJ, et al. Increased stiffness of the tumor microenvironment in colon cancer stimulates cancer associated fibroblast-mediated prometastatic activin a signaling. Sci Rep. 2020;10 (1):50. doi: 10.1038/s41598-019-55687-6

[126] Kaukonen R, Mai A, Georgiadou M, et al. Normal stroma suppresses cancer cell proliferation via mechanosensitive regulation of JMJD1a-mediated transcription. Nat Commun. 2016;7(1):12237. doi: 10.1038/ncomms12237

[127] Liu C, Liu Y, Xie HG, et al. Role of three-dimensional matrix stiffness in regulating the chemoresistance of hepatocellular carcinoma cells. Biotechnol Appl Biochem. 2015;62(4):556–562. doi: 10.1002/bab.1302

[128] Lv Y, Wang H, Li G, et al. Three-dimensional decellularized tumor extracellular matrices with different stiffness as bioengineered tumor scaffolds. Bioact Mater. 2021;6(9):2767–2782. doi: 10.1016/j.bioact mat.2021.02.004

[129] Ma X, Yu C, Wang P, et al. Rapid 3D bioprinting of decellularized extracellular matrix with regionally varied mechanical properties and biomimetic microarchitecture. Biomaterials. 2018;185:310–321. doi: 10.1016/j.biomaterials.2018.09.026

[130] Gao S, Guo W, Chen M, et al. Fabrication and characterization of electrospun nanofibers composed of decellularized meniscus extracellular matrix and polycaprolactone for meniscus tissue engineering. J Mater Chem B. 2017;5(12):2273–2285. doi: 10.1039/C6TB03299K

[131] Peng X, Kristi N, Gafur A, et al. Micromechanical property analyses of decellularized vessels by atomic

force microscopy. J Phys D Appl Phys. 2019;52 (42):425401. doi: 10.1088/1361-6463/ab33ce

[132] Mendoza-Novelo B, Avila EE, Cauich-Rodríguez JV, et al. Decellularization of pericardial tissue and its impact on tensile viscoelasticity and glycosaminoglycan content. Acta Biomater. 2011;7(3):1241–1248. doi: 10.1016/j.actbio.2010.11.017

[133] Williams C, Liao J, Joyce EM, et al. Altered structural and mechanical properties in decellularized rabbit carotid arteries. Acta Biomater. 2009;5(4):993–1005. doi: 10.1016/j.actbio.2008.11.028

[134] Luque T, Melo E, Garreta E, et al. Local micromechanical properties of decellularized lung scaffolds measured with atomic force microscopy. Acta Biomater. 2013;9(6):6852–6859. doi: 10.1016/j.act bio.2013.02.044

[135] Holuigue H, Nacci L, Di Chiaro P, et al. Native extracellular matrix probes to target patient-and tissue-specific cell–microenvironment interactions by force spectroscopy. Nanoscale. 2023;15 (37):15382–15395. doi: 10.1039/D3NR01568H

[136] Petrou CL, D'Ovidio TJ, Bölükbas DA, et al. Clickable decellularized extracellular matrix as a new tool for building hybrid-hydrogels to model chronic fibrotic diseases in vitro. J Mater Chem B. 2020;8 (31):6814–6826. doi: 10.1039/D0TB00613K

[137] Xu J, Fang Q, Liu Y, et al. In situ ornamenting poly (ε-caprolactone) electrospun fibers with different fiber diameters using chondrocyte-derived extracellular matrix for chondrogenesis of mesenchymal stem cells. Colloids Surf B Biointerfaces. 2021;197:111374. doi: 10.1016/j.colsurfb.2020.111374

[138] Ghorbani F, Moradi L, Shadmehr MB, et al. In-vivo characterization of a 3D hybrid scaffold based on PCL/decellularized aorta for tracheal tissue engineering. Mater Sci Eng C Mater Biol Appl. 2017;81:74–83. doi: 10.1016/j.msec.2017.04.150

[139] Ergun C, Parmaksiz M, Vurat MT, et al. Decellularized liver ecm-based 3D scaffolds: compositional, physical, chemical, rheological, thermal, mechanical, and in vitro biological evaluations. Int J Biol Macromol. 2022;200:110–123. doi: 10. 1016/j.ijbiomac.2021.12.086

[140] Lee H, Ju YM, Kim I, et al. A novel decellularized skeletal muscle-derived ECM scaffolding system for in situ muscle regeneration. Methods. 2020;171:77–85. doi: 10.1016/j.ymeth.2019.06.027

[141] Lacueva-Aparicio A, Lindoso RS, Mihăilă SM, et al. Role of extracellular matrix components and structure in new renal models in vitro. Front Physiol. 2022;13:1048738. doi: 10.3389/fphys.2022.1048738